

A Residual A Posteriori error estimate for the Virtual Element Method

Original

A Residual A Posteriori error estimate for the Virtual Element Method / Berrone, Stefano; Borio, Andrea. - In: MATHEMATICAL MODELS AND METHODS IN APPLIED SCIENCES. - ISSN 0218-2025. - STAMPA. - 27:8(2017), pp. 1423-1458. [10.1142/S0218202517500233]

Availability:

This version is available at: 11583/2666363 since: 2017-03-03T11:02:20Z

Publisher:

World Scientific Publishing Company

Published

DOI:10.1142/S0218202517500233

Terms of use:

This article is made available under terms and conditions as specified in the corresponding bibliographic description in the repository

Publisher copyright

(Article begins on next page)

A Residual A Posteriori error estimate for the Virtual Element Method*

Stefano Berrone

*Dipartimento di Scienze Matematiche, Politecnico di Torino, Corso Duca degli Abruzzi 24
Torino, 10129, Italy
stefano.berrone@polito.it*

Andrea Borio

*Dipartimento di Scienze Matematiche, Politecnico di Torino, Corso Duca degli Abruzzi 24
Torino, 10129, Italy
andrea.borio@polito.it*

A residual based a posteriori error estimate for the Poisson problem with discontinuous diffusivity coefficient is derived in the case of a Virtual Element discretization. The error is measured considering a suitable polynomial projection of the discrete solution to prove an equivalence between the defined error and a computable residual based error estimator that does not involve any term related to the Virtual Element stabilization. Numerical results display a very good behaviour of the ratio between the error and the error estimator, resulting independent of the meshsize and element distortion.

Keywords: “A posteriori” error estimates; Virtual Element Method; mesh adaptivity; Single-phase flows; underground flow simulations

AMS Subject Classification: 65N15, 65N30, 65N50, 86-08, 86A05

1. Introduction

Since the first investigations on a *posteriori* error analysis,⁶ many interesting results have been obtained^{46,3,7,39} on simple linear models as well as on more complex non-linear equations.^{20,31,27} In recent years a *posteriori* error analysis and optimality investigations of steady-state adaptive discretizations have been widely tackled for several discretization approaches and model equations, obtaining several interesting results.^{32,43,36,26} A large effort has been recently spent on unsteady problems,^{47,4,23,37} as well as on other interesting issues like, for example, the analysis of stopping criteria during adaptive iterations.⁴⁰ Discretization approaches based on traditional simplicial elements are subject to many constraints when mesh refinement and coarsening are applied. These constraints can make reliable and efficient

*This research has been partially supported by the Italian MIUR through PRIN research grant 2012HBLYE4.001 *Metodologie innovative nella modellistica differenziale numerica* and by INdAM-GNCS. Computational resources were provided by HPC@POLITO (<http://www.hpc.polito.it>).

simulations very difficult and computationally demanding. Moreover, in many applications the geometrical complexity of the domain is a relevant issue when partial differential equations have to be solved on a good quality mesh (see, for example, the problem of underground flow simulation in fractured media^{28,30,29}).

The Virtual Element Method (VEM)⁸ was recently developed as a generalization of Mimetic Finite Differences,^{33,11} with the main target to overcome traditional simplicial discretizations in 2D and in 3D and allow the use of an arbitrary polytopal mesh, allowing, for examples, also polygons with different number of edges in 2D. VEM discretizations require only some basic regularity assumptions on the mesh elements, at the price of enlarging the standard polynomial spaces to include some additional basis functions, whose expression is never to be explicitly evaluated. Stability, consistency and polynomial approximation properties are provided by a suitable choice of the degrees of freedom and by suitable stabilization terms of the discrete bilinear form. The VEM is currently under continuous development, in order to deal with a larger and larger number of models, including primal and mixed formulations. Due to the unknown value of the non-polynomial part of the discretization space on each element, the computed discrete solution is immediately known only through the values of its degrees of freedom and not easily evaluated inside the elements. The full discrete solution can, however, be used to compute a piecewise polynomial approximation of the discrete solution that can be easily evaluated at any point of each element.

In this work we address the issue of deriving computable, reliable and efficient residual-based *a posteriori* error estimators for a polynomial projection of the Virtual Element solution to the Poisson problem. This very simple model is, anyway, interesting in several applications like, for example, geological flow simulations^{28,17,18,15} where the geometrical complexities can be extremely challenging. The *a posteriori* analysis for the same problem was tackled in Ref. 14 with a different VEM discretization and with additional terms in the estimates depending on the VEM stabilization. Moreover, in Ref. 34 a more general reaction-advection-diffusion problem is considered for an *a posteriori* error estimate, involving terms depending on the VEM stabilization. In Ref. 16 a SUPG-like stabilization is introduced for a convection dominated advection-diffusion flow. Here we show that, using a particular polynomial approximation of the VEM solution, we are able to compute reliable and efficient residual error estimators, overcoming the problem related to the evaluation of the residual of the strong form of the equation and of the values of the co-normal derivatives of the non-polynomial component of the numerical solution. Moreover, we aim at avoiding the inclusion in the error estimators of any VEM stabilization terms. In this approach, we assume the existence of an oblique projection operator in Definition 3.2, whose stability is addressed numerically in Appendix. Under this assumption, we establish an equivalence relation between the error with respect to a “post-processing” of the VEM solution and a residual based error estimator. Resorting to post-processed solutions is a quite common practice in proving super-convergence results,^{51,49} very common, for example, for the Stokes

problem.⁵⁰ The equivalence relation we prove involves only the defined error measure and the error estimator, up to classical higher order data oscillation terms. Note that, in the case the estimates were not independent of the VEM stabilization, as they are with other approaches, one would have these terms, that are not negligible with respect to the error and the estimator, on the right-hand side of both the upper and lower bound of the error.

The paper is organized as follows: in Sec. 2.1 we describe the model problem, in Sec. 2.2 we briefly introduce the VEM conforming discretization. In Sec. 3 the *a posteriori* upper bound for the error between the solution of the problem and a suitable projection of the numerical solution is provided, and in Sec. 4 we prove *a posteriori* lower bounds for the chosen error measure. In Sec. 5 we present some numerical results confirming the good behaviour of the *a posteriori* error estimates. In particular, we show that the estimates can be effectively applied to a model representing the pressure distribution of a Darcy flow within a fractured medium, modeled by a Discrete Fracture Network approach.^{28,30,29,25,18,15} Finally, in Appendix 7 we discuss a stability issue concerning a fundamental assumption needed in order to have estimates independent of the VEM stabilization terms.

In the paper, for sake of clarity, we consider the 2D case only, we remark that all the results concerning the *a posteriori* error estimates presented in Sections 3 and 4 can be extended to the 3D case as well.

2. The model problem and its VEM discretization

In this section we introduce the problem which will be considered herein, followed by its discretization by the Virtual Element Method, that follows the lines developed in Ref. 10.

2.1. The model problem

In the present work we consider the simple Poisson problem. Let $\Omega \subset \mathbb{R}^2$ be a bounded open set with Lipschitz boundary $\partial\Omega$; then, for a forcing term f we look for a function u such that

$$\begin{cases} -\nabla \cdot (\kappa \nabla u) = f & \text{in } \Omega, \\ u = 0 & \text{on } \partial\Omega, \end{cases} \quad (2.1)$$

where κ is a positive function representing the *diffusivity* coefficient. We consider the classic weak formulation of the problem: let $a : H_0^1(\Omega) \times H_0^1(\Omega) \rightarrow \mathbb{R}$ be such that

$$a(w, v) := (\kappa \nabla w, \nabla v) \quad \forall w, v \in H_0^1(\Omega),$$

where (\cdot, \cdot) is the $L^2(\Omega)$ scalar product, $\kappa \in L^\infty(\Omega)$ and $f \in L^2(\Omega)$. The variational form of (2.1) is: find $u \in H_0^1(\Omega)$ such that

$$a(u, v) = (f, v) \quad \forall v \in H_0^1(\Omega). \quad (2.2)$$

2.2. VEM discretization

The Virtual Element Method is a quite recent discretization approach and its extensions to more complex models than the one considered here are currently largely investigated.^{35,5,12}

Let \mathcal{T}_h be a discretization of $\Omega \subset \mathbb{R}^2$ with open star-shaped polygons having an arbitrary number of sides (even different from one polygon to another) and let \mathcal{E}_h be the set of their edges. As a regularity assumption, we assume that $\forall E \in \mathcal{T}_h$, with diameter h_E , there exists a constant $\gamma > 0$ such that

- E is star-shaped with respect to a ball B_E of radius larger than γh_E ;
- for any two vertices $\mathbf{x}_1, \mathbf{x}_2 \in E$, $\|\mathbf{x}_1 - \mathbf{x}_2\|_{\mathbb{R}^2} \geq \gamma h_E$.

Thanks to this assumption, it is possible to construct, on each element $E \in \mathcal{T}_h$, a uniformly shape regular nested triangulation $\mathcal{T}_{h,E}$ whose triangles t are such that

$$\forall E \in \mathcal{T}_h, \forall t \in \mathcal{T}_{h,E}, \quad h_E \geq h_t \geq \gamma h_E, \quad (2.3)$$

and each of these triangles have one edge lying on ∂E . This can be accomplished, for example, by connecting all vertices of E to the center of the ball B_E , whose coordinates are $\mathbf{x}_E = (x_E, y_E)$. Now, consider an edge $e \in \mathcal{E}_h$ and let $R, L \in \mathcal{T}_h$ be the two polygons sharing e . Let $r \in \mathcal{T}_{h,R}$ and $l \in \mathcal{T}_{h,L}$ be the two triangles contained in L and R respectively and sharing e , we set $\Omega_e := \{R, L\}$ and $\omega_e := \{r, l\}$.

We now turn to the definition of the virtual spaces. Let $k \in \mathbb{N}$ be the ‘‘polynomial order’’ of the VEM discretization. First of all, we introduce an oblique projection.⁸ Let $\Pi_k^\nabla : H_0^1(\Omega) \rightarrow \mathbb{P}_k(\mathcal{T}_h)$ be the operator such that, $\forall v \in H_0^1(\Omega)$ and $\forall E \in \mathcal{T}_h$,

$$(\nabla(v - \Pi_k^\nabla v), \nabla p)_E = 0, \forall p \in \mathbb{P}_k(E) \quad \text{and} \quad \begin{cases} (\Pi_k^\nabla v, 1)_{\partial E} = (v, 1)_{\partial E} & \text{if } k = 1, \\ (\Pi_k^\nabla v, 1)_E = (v, 1)_E & \text{if } k \geq 1, \end{cases}$$

where $\mathbb{P}_k(\omega)$ is the space of the polynomials of degree less than or equal to k on ω . Following Ref. 10, we introduce the finite dimensional spaces

$$\begin{aligned} V_h^E &= \{v \in H^1(E) : \Delta v \in \mathbb{P}_k(E), v \in \mathbb{P}_k(e) \forall e \subset \partial E, \gamma_{\partial E}(v) \in C^0(\partial E), \\ &\quad (v, p)_E = (\Pi_k^\nabla v, p)_E \forall p \in \mathbb{P}_k(E) / \mathbb{P}_{k-2}(E)\}, \quad \forall E \in \mathcal{T}_h, \\ V_h &= \{v \in C^0(\Omega) \cap H_0^1(\Omega) : v \in V_h^E \forall E \in \mathcal{T}_h\}, \end{aligned}$$

where $\mathbb{P}_k(E) / \mathbb{P}_{k-2}(E)$ denotes the subspace of $\mathbb{P}_k(E)$ containing polynomials that are $L^2(E)$ -orthogonal to $\mathbb{P}_{k-2}(E)$ (see Ref. 10; other options are possible, see, for example, Ref. 2).

Definition 2.1. A function $v \in V_h$ can be described on each polygon $E \in \mathcal{T}_h$ by the following degrees of freedom:

- (1) the values at the vertices of the polygon;
- (2) if $k \geq 2$, for each edge $e \subset \partial E$, the value of v at $k - 1$ internal points of e . For practical purposes, we choose these points to be the internal Gauss – Lobatto quadrature nodes;

- (3) if $k \geq 2$, the moments $(v, m_{\alpha})_E$ for all the monomials up to the order $k - 2$ $m_{\alpha} \in \mathcal{M}_{k-2}(E)$, with $\alpha = (\alpha_1, \alpha_2)$, $|\alpha| = \alpha_1 + \alpha_2 \leq k - 2$, and

$$\forall \mathbf{x} = (x, y) \in E, \quad m_{\alpha}(x, y) := \frac{(x - x_E)^{\alpha_1} (y - y_E)^{\alpha_2}}{h_E^{\alpha_1 + \alpha_2}}. \quad (2.4)$$

We point out that the just stated degrees of freedom uniquely identify the polynomial expression of a function in V_h on each edge of the discretization, whereas inside the polygons these functions can not be directly evaluated. The above degrees of freedom are enough to compute, for any $v_h \in V_h$, the projection $\Pi_k^{\nabla} v_h$, see Ref. 9, and, once it is known, to compute the $L^2(\Omega)$ projection of v_h on $\mathbb{P}_k(\mathcal{T}_h)$, which is indicated by $\Pi_k^0 v_h$ in the following. Similarly, $\Pi_{k-1}^0 \nabla v_h$ indicates the vector containing the $L^2(\Omega)$ projection on $\mathbb{P}_{k-1}(\mathcal{T}_h)$ of the partial derivatives of v_h , which is computable using the degrees of freedom, see Ref. 10.

To introduce the VEM discretization of the Poisson problem we suppose to know, for each $E \in \mathcal{T}_h$, a symmetric bilinear form $S^E: V_h \times V_h \rightarrow \mathbb{R}$ that scales like a^E on the kernel of Π_k^{∇} , i.e. $\exists c_*, c^* > 0$ such that

$$\forall v_h \in V_h \text{ with } \Pi_k^{\nabla} v_h = 0, \quad c_* a^E(v_h, v_h) \leq S^E(v_h, v_h) \leq c^* a^E(v_h, v_h), \quad (2.5)$$

where $a^E(v, w) := (\kappa \nabla v, \nabla w)_E$. Once S^E is given, we can define the following local and global discrete bilinear forms:

$$\begin{aligned} \forall E \in \mathcal{T}_h, \forall u_h, v_h \in V_h, \quad a_h^E(u_h, v_h) &:= (\kappa \Pi_{k-1}^0 \nabla u_h, \Pi_{k-1}^0 \nabla v_h)_E \\ &\quad + S^E((I - \Pi_k^{\nabla}) u_h, (I - \Pi_k^{\nabla}) v_h), \\ \forall u_h, v_h \in V_h, \quad a_h(u_h, v_h) &:= \sum_{E \in \mathcal{T}_h} a_h^E(u_h, v_h). \end{aligned}$$

With the above definitions, we can formulate the Virtual Element method as the solution to the following discrete problem: find $u_h \in V_h$ such that

$$a_h(u_h, v_h) = (f_h, v_h) \quad \forall v_h \in V_h, \quad (2.6)$$

where $f_h := \Pi_k^0 f$, that is the best approximation of f that allows the computability of the scalar product with a VEM function, since $(\Pi_k^0 f, v_h) = (f, \Pi_k^0 v_h)$ and we can compute $\Pi_k^0 v_h$ using the degrees of freedom. The well-posedness of this problem simply follows by noticing that, thanks to (2.5), a_h is coercive on V_h ; optimal orders of convergence are proved in Ref. 10.

Remark 2.1. One possible choice for S^E (see Ref. 8) is the scalar product between the two vectors containing the degrees of freedom of the two functions involved, i.e., if we indicate by χ_r the operator which associates to each function in V_h its r -th degree of freedom,

$$S^E(u_h, v_h) := \sum_{r=1}^{N_E} \chi_r(u_h) \chi_r(v_h) \quad \forall E \in \mathcal{T}_h, \forall u_h, v_h \in V_h, \quad (2.7)$$

where N_E indicates the number of degrees of freedom on element E . A detailed discussion of mesh assumptions and other stabilization operators can be found in Ref. 13.

3. A residual a posteriori estimate

In the following we derive *a posteriori* error estimates for a post-processing of the VEM solution to problem (2.6). A common issue when dealing with a VEM solution u_h is related to the difficulties in getting pointwise values internal to the elements, for example to compute integrals or gradients of the solutions for the computation of some physically relevant quantities (maximum or minimum value of the solution, fluxes, stresses). This problem is quite commonly tackled by means of pointwise evaluation of suitable projected solutions.¹² For this reason we have chosen to evaluate the error between the exact solution u and a polynomial projection of the computed VEM solution in order to have a control on the quality of the solution we are using for the given applicative targets. Indeed, in the following we show that, if a suitable polynomial approximation of u_h , solution to (2.6), is considered, classical error estimation techniques can be applied to obtain computable, reliable and efficient upper and lower bounds.

We will use the notations \lesssim and \sim to indicate inequalities or equivalences up to multiplicative constants independent of the meshsize and the diffusivity coefficient:

$$\forall a, b \in \mathbb{R}, a \lesssim b \iff \exists c > 0: a \leq cb \text{ and } a \sim b \iff \exists c_1, c_2 > 0: c_1 b \leq a \leq c_2 b.$$

Assumption 1. From now on we assume that κ is piecewise constant on \mathcal{T}_h and set $\kappa_E := \kappa|_E$, for any given element $E \in \mathcal{T}_h$. Furthermore, for a given set of elements ω , we set $\kappa_\omega^\wedge := \max_\omega \kappa$ and $\kappa_\omega^\vee := \min_\omega \kappa$.

3.1. Post-processing of the discrete solution and error definition

For any $v_h \in V_h$, we define the piecewise discontinuous polynomial function v_h^π , that, on each $E \in \mathcal{T}_h$, is the solution to the local problem

$$(\kappa \nabla v_h^\pi, \nabla p)_E = (\kappa \Pi_{k-1}^0 \nabla v_h, \nabla p)_E \quad \forall p \in \mathbb{P}_k(E) \quad \text{and} \quad (v_h^\pi, 1)_{\partial E} = (v_h, 1)_{\partial E}. \quad (3.1)$$

Remark 3.1. Since here we are considering a piecewise constant diffusivity, we can remove κ and Π_{k-1}^0 from (3.1). In this case, $v_h^\pi = \Pi_k^\nabla v_h$, i.e. the definition of (3.1) is equivalent to the definition of the operator Π_k^∇ . In the case of non-elementwise constant κ , (3.1) has to be used and additional terms will appear in the estimate, as described in Remark 3.7.

We will estimate the error between the exact solution to problem (2.1) and this post-processing of the discrete solution:

$$e_h^\pi := u - u_h^\pi.$$

Since u_h^π is not continuous, we need to define a broken semi-norm:

$$\|v\| := \sup_{w \in H_0^1(\Omega)} \frac{\sum_{E \in \mathcal{T}_h} a^E(v, w)}{\|\sqrt{\kappa} \nabla w\|}. \quad (3.2)$$

Remark 3.2. We point out that the semi-norm $\|\cdot\|$ is a norm for the error $e_h^\pi \in \prod_{E \in \mathcal{T}_h} H^1(E)$ even though u_h^π does not vanish on the boundary $\partial\Omega$ as u does, because $\|e_h^\pi\| = 0$ implies $e_h^\pi = 0$ in Ω . In fact, suppose $\|u - u_h^\pi\| = 0$, then, it must hold $(\nabla u - \nabla u_h^\pi)|_E = 0, \forall E \in \mathcal{T}_h$, implying

$$\forall E \in \mathcal{T}_h, (u - u_h^\pi)|_E = C_E \in \mathbb{R} \Rightarrow u|_E = u_h^\pi|_E + C_E \in \mathbb{P}_k(E).$$

Then, it follows that $u|_E \in \mathbb{P}_k(E), \forall E \in \mathcal{T}_h$, and $u \in V_h$. Then, one has $u = u_h = u_h^\pi$, which means that $C_E = 0 \forall E \in \mathcal{T}_h$. We conclude that $\|u - u_h^\pi\| = 0 \iff u - u_h^\pi = 0$.

We have the following a priori estimate of the error e_h^π .

Theorem 3.1. *Suppose κ is piecewise constant on \mathcal{T}_h , $u \in H^{s+1}(\Omega)$ for some $s > 0$, where k is the order of the VEM approximation. Then, if $r = \min\{k, s\}$,*

$$\exists C > 0: \|u - u_h^\pi\|^2 \lesssim \sum_{E \in \mathcal{T}_h} \kappa_E h_E^{2r} |u|_{H^{r+1}(E)}^2$$

Proof. By the triangle inequality, the continuity of Π_k^∇ and VEM convergence estimates, we have

$$\|u - u_h^\pi\|^2 \leq \|u - \Pi_k^\nabla u\|^2 + \|\Pi_k^\nabla(u - u_h)\|^2 \lesssim \sum_{E \in \mathcal{T}_h} \kappa_E h_E^{2r} |u|_{H^{r+1}(E)}^2. \quad \square$$

The above result shows that the error e_h^π has the same order of convergence as the error $u - u_h$. Thus, an efficient a posteriori estimate for e_h^π will have the same order of convergence as $u - u_h$.

3.2. A posteriori upper bound

Before proceeding to the major result, we need to build a locally continuous linear operator that will play the same role as the Clément pseudo-interpolator in the standard FEM context (see Ref. 46).

3.2.1. An oblique projection operator

In the following we focus on the VEM stabilization (2.7) (see Ref. 8).

Let $u_h \in V_h$ be the solution to (2.6) and let

$$W_h := \{v_h \in V_h: S((I - \Pi_k^\nabla)u_h, (I - \Pi_k^\nabla)v_h) = 0\}.$$

Definition 3.1. Let $\mathcal{T}_{h,\omega}$ be a partition of Ω such that each element $\omega \in \mathcal{T}_{h,\omega}$ is:

- (1) the union of elements $E \in \mathcal{T}_h$, and each element E is contained in one and only one of such ω ;
- (2) a set of elements $E \in \mathcal{T}_h$ with a uniformly bounded number of elements;
- (3) a Lipschitz set whose diameter scales as the diameter of its elements;
- (4) either $(I - \Pi_k^\nabla)u_h = 0 \forall E \in \omega$, or there is at least one degree of freedom of the space V_h whose corresponding basis function φ_r satisfy $\text{supp } \varphi_r \subseteq \omega$ and

$$\sum_{E \in \omega} S^E ((I - \Pi_k^\nabla) u_h, (I - \Pi_k^\nabla) \varphi_r) \neq 0. \quad (3.3)$$

Let us denote by V_h^ω the space of the restrictions to ω of VEM functions in V_h . Given $\mathcal{T}_{h,\omega}$, we can build an oblique projection as follows.

Definition 3.2. Let $\mathcal{S}_h^\omega: V_h^\omega \rightarrow W_h^\omega$ be a linear continuous operator, defined locally, such that, for any given $v \in V_h^\omega$ and any $\omega \in \mathcal{T}_{h,\omega}$,

- (1) for all the VEM dofs s (Definition 2.1) of the elements E in the patch ω , except for $s = r$ only if $(I - \Pi_k^\nabla)u_h|_\omega \neq 0$,

$$\chi_s(\mathcal{S}_h^\omega v) = \chi_s(v);$$

- (2) it holds

$$\sum_{E \in \omega} S^E ((I - \Pi_k^\nabla) u_h, (I - \Pi_k^\nabla) \mathcal{S}_h^\omega v) = 0, \quad (3.4)$$

i.e. the r -th degree of freedom $\chi_r(\mathcal{S}_h^\omega v)$ is chosen to satisfy (3.4) if $(I - \Pi_k^\nabla)u_h|_\omega \neq 0$.

Remark 3.3. Whenever $v \in V_h$ is constant on $\omega \in \mathcal{T}_{h,\omega}$, condition (3.4) is automatically satisfied and \mathcal{S}_h^ω is the identity on ω . We conclude that the operator \mathcal{S}_h^ω preserves local constant functions on ω .

Definition 3.3. (Ref. 34) Let $I_h: H^1(\Omega) \rightarrow V_h$ be a VEM interpolation operator such that, $\forall E \in \mathcal{T}_h$,

$$\|v - I_h v\|_E \lesssim h_E \|\nabla v\|_{\tilde{E}}, \quad (3.5)$$

$$\|\nabla I_h v\|_E \lesssim \|\nabla v\|_{\tilde{E}}, \quad (3.6)$$

where \tilde{E} is the set of polygons with non-empty intersection with E .

The existence of such operator is guaranteed by Theorem 11 in Ref. 34 under the regularity hypothesis made in Section 2.2 by which we can build a uniformly shape regular triangulation on each polygon.

Definition 3.4. Let \mathcal{S}_h^ω be the operator defined by Definition 3.2, and I_h be the operator defined by Definition 3.3. We define $P_h^\omega: H^1(\Omega) \rightarrow W_h^\omega$ (restriction of W_h to ω) such that $P_h^\omega := \mathcal{S}_h^\omega \circ R_h^\omega \circ I_h$, where R_h^ω is the restriction operator from V_h to V_h^ω . The operator $P_h: H^1(\Omega) \rightarrow W_h$ is defined such that $P_h v|_\omega := P_h^\omega v$, $\forall v \in H^1(\Omega)$, $\forall \omega \in \mathcal{T}_{h,\omega}$.

Let \mathcal{E}_h be the set of the edges of the VEM mesh not on the boundary of Ω .

Definition 3.5. For each $E \in \mathcal{T}_h$, we indicate by ω_E the patch of elements to which it uniquely belongs, and by $\tilde{\omega}_E$ the patch of elements sharing at least one vertex with ω_E . Moreover, for each $e \in \mathcal{E}_h$, we set $\tilde{\omega}_e := \cup_{E \in \Omega_e} \tilde{\omega}_E$, where Ω_e is the set of elements sharing e , as defined in Section 2.2.

Definition 3.6. For each internal edge $e \in \mathcal{E}_h$ let

$$\kappa_e := \sum_{E \in \Omega_e} \kappa_E$$

be the diffusivity associated to e .

The operator P_h satisfies the following important bounds.

Lemma 3.1. *Let P_h be defined by Definition 3.4. Then, $\forall v \in H_0^1(\Omega)$,*

$$\|v - P_h v\|_E \lesssim h_E \|\nabla v\|_{\tilde{\omega}_E} \quad \forall E \in \mathcal{T}_h, \quad (3.7)$$

$$\|\nabla(v - P_h v)\|_E \lesssim \|\nabla v\|_{\tilde{\omega}_E} \quad \forall E \in \mathcal{T}_h, \quad (3.8)$$

$$\|v - P_h v\|_e \lesssim h_e^{\frac{1}{2}} \|\nabla v\|_{\tilde{\omega}_e} \quad \forall e \in \mathcal{E}_h, \quad (3.9)$$

$$\|v - P_h v\|_E \lesssim C_{\kappa, E} \frac{h_E}{\sqrt{\kappa_E}} \|\sqrt{\kappa} \nabla v\|_{\tilde{\omega}_E} \quad \forall E \in \mathcal{T}_h, \quad (3.10)$$

$$\|v - P_h v\|_e \lesssim C_{\kappa, e} \frac{h_e^{\frac{1}{2}}}{\sqrt{\kappa_e}} \|\sqrt{\kappa} \nabla v\|_{\tilde{\omega}_e} \quad \forall e \in \mathcal{E}_h, \quad (3.11)$$

$C_{\kappa, E}$ and $C_{\kappa, e}$ being constants depending only on the jumps of κ .

Proof. Let $v \in H^1(\Omega)$ and $v_I := I_h v$. First, we observe that, thanks to (3.5), we have

$$\|v - P_h v\|_E \lesssim \|v - v_I\|_E + \|v_I - \mathcal{S}_h^{\omega_E} v_I|_{\omega_E}\|_E \lesssim h_E \|\nabla v\|_{\hat{E}} + \|v_I - \mathcal{S}_h^{\omega_E} v_I|_{\omega_E}\|_{\omega_E}.$$

We are left to estimate the second norm. Let \hat{E} be a polygon with $h_{\hat{E}} \simeq 1$ such that the element E is obtained by a isotropic rescaling $E = F_E(\hat{E})$, and let $\hat{\omega}_E$ be the Lipschitz set such that $\omega_E = F_E(\hat{\omega}_E)$. Let us prove that there exists a constant $C_{\hat{E}}$ such that, for any $v \in V_h$ and any $E \in \mathcal{T}_h$,

$$\left\| \hat{v} - \mathcal{S}_h^{\hat{\omega}_E} \hat{v} \right\|_{\hat{\omega}_E} \leq C_{\hat{E}} \|\nabla \hat{v}\|_{\hat{\omega}_E}, \quad (3.12)$$

where from now on with \hat{v} we mean $(v \circ F_E)|_{\hat{\omega}_E}$. We suppose by contradiction that for any $C > 0$ there exists a $v \in V_h$ such that

$$\left\| \hat{v} - \mathcal{S}_h^{\hat{\omega}_E} \hat{v} \right\|_{\hat{\omega}_E} > C \|\nabla \hat{v}\|_{\hat{\omega}_E},$$

in which case we can build a sequence w_k of functions in V_h such that $\hat{w}_k = (w_k \circ F_E)|_{\hat{\omega}_E}$ and

$$\left\| \hat{w}_k - \mathcal{S}_h^{\hat{\omega}_E} \hat{w}_k \right\|_{L^2(\hat{\omega}_E)} \geq k \|\nabla \hat{w}_k\|_{L^2(\hat{\omega}_E)}, \quad \left\| \hat{w}_k - \mathcal{S}_h^{\hat{\omega}_E} \hat{w}_k \right\|_{L^2(\hat{\omega}_E)} = 1,$$

10

which means that

$$\|\nabla \hat{w}_k\|_{L^2(\hat{\omega}_E)} \leq \frac{1}{k} \Rightarrow \|\nabla \hat{w}_k\|_{L^2(\hat{\omega}_E)} \rightarrow 0.$$

Then, if we define $\hat{u}_k = \hat{w}_k - \mathcal{S}_h^{\hat{\omega}_E} \hat{w}_k$, we have, by the continuity of $\mathcal{S}_h^{\hat{\omega}_E}$ for any given patch and u_h , and the fact that it preserves constants, that, if \hat{w}_k tends to a constant, also $\mathcal{S}_h^{\hat{\omega}_E} \hat{w}_k$ tends to the same constant. Then,

$$\|\nabla \hat{u}_k\|_{L^2(\hat{\omega}_E)} \rightarrow 0. \quad (3.13)$$

The sequence $\hat{u}_k \circ F_E^{-1} \in V_h^{\omega_E} \cap H_0^1(\omega_E)$ and $\|\hat{u}_k\|_{L^2(\hat{\omega}_E)} = 1$, thus it converges to a function \hat{u}^* up to sub-sequences. By (3.13), $\nabla \hat{u}^* = 0$, thus \hat{u}^* is constant and it must be $\hat{u}^* = 0$ being $\hat{u}^*|_{\partial \hat{\omega}_E} = 0$. This is a contradiction since $\|\hat{u}^*\|_{\hat{\omega}_E} = 1$. We conclude that (3.12) must hold and, by scaling arguments and (3.6), we get

$$\|v_I - \mathcal{S}_h^{\omega_E} v_I|_{\omega_E}\|_{\omega_E} \lesssim h_E \|\nabla v_I\|_{\tilde{\omega}_E} \lesssim h_E \|\nabla v\|_{\tilde{\omega}_E}.$$

By similar arguments we get also (3.8). Considering

$$\begin{aligned} \|\nabla v\|_{\tilde{\omega}_E} &\lesssim \frac{1}{\sqrt{\kappa_{\tilde{\omega}_E}^\vee}} \|\sqrt{\kappa} \nabla v\|_{\omega_E} \lesssim \frac{\sqrt{\kappa_E}}{\sqrt{\kappa_{\tilde{\omega}_E}^\vee}} \frac{1}{\sqrt{\kappa_E}} \|\sqrt{\kappa} \nabla v\|_{\omega_E} \leq \\ &\leq \frac{\sqrt{\kappa_{\tilde{\omega}_E}^\wedge}}{\sqrt{\kappa_{\tilde{\omega}_E}^\vee}} \frac{1}{\sqrt{\kappa_E}} \|\sqrt{\kappa} \nabla v\|_{\tilde{\omega}_E}, \end{aligned}$$

we get (3.10).

Regarding (3.9) and (3.11), we apply a trace inequality, (3.7) and (3.8). Let $e \in \mathcal{E}_h$ and $E \in \Omega_e$:

$$\begin{aligned} \|v - P_h v\|_e^2 &\lesssim h_e^{-1} \|v - P_h v\|_E^2 + h_e \|\nabla(v - P_h v)\|_E^2 \lesssim h_e^{-1} h_E^2 \|\nabla v\|_{\tilde{\omega}_E}^2 \\ &\quad + h_e \|\nabla v\|_{\tilde{\omega}_E}^2 \lesssim h_e \|\nabla v\|_{\tilde{\omega}_E}^2 \lesssim \frac{\kappa_{\tilde{\omega}_E}^\wedge}{\kappa_{\tilde{\omega}_E}^\vee} \frac{h_e}{\kappa_E} \|\sqrt{\kappa} \nabla v\|_{\tilde{\omega}_E}^2, \end{aligned}$$

because $h_E \lesssim h_e$ by mesh regularity assumptions. To complete the proof of (3.11), we denote $\Omega_e = \{R, L\}$ and use the above estimate, bearing in mind that κ is constant on both R and L :

$$\begin{aligned} \kappa_R \|v - P_h v\|_e^2 &\lesssim \frac{\kappa_{\tilde{\omega}_R}^\wedge}{\kappa_{\tilde{\omega}_R}^\vee} h_e \|\sqrt{\kappa} \nabla v\|_{\tilde{\omega}_R}^2, \quad \kappa_L \|v - P_h v\|_e^2 \lesssim \frac{\kappa_{\tilde{\omega}_L}^\wedge}{\kappa_{\tilde{\omega}_L}^\vee} h_e \|\sqrt{\kappa} \nabla v\|_{\tilde{\omega}_L}^2 \\ &\Rightarrow (\kappa_R + \kappa_L) \|v - P_h v\|_e^2 \lesssim \max \left\{ \frac{\kappa_{\tilde{\omega}_R}^\wedge}{\kappa_{\tilde{\omega}_R}^\vee}, \frac{\kappa_{\tilde{\omega}_L}^\wedge}{\kappa_{\tilde{\omega}_L}^\vee} \right\} h_e \|\sqrt{\kappa} \nabla v\|_{\tilde{\omega}_e}^2 \\ &\Rightarrow \|v - P_h v\|_e^2 \lesssim \max \left\{ \frac{\kappa_{\tilde{\omega}_R}^\wedge}{\kappa_{\tilde{\omega}_R}^\vee}, \frac{\kappa_{\tilde{\omega}_L}^\wedge}{\kappa_{\tilde{\omega}_L}^\vee} \right\} \frac{h_e}{\kappa_e} \|\sqrt{\kappa} \nabla v\|_{\tilde{\omega}_e}^2. \quad \square \end{aligned}$$

Remark 3.4. $\forall e \in \mathcal{E}_h$, if $C_{\kappa, E} = 1$, for all $E \in \tilde{\omega}_e$, then $C_{\kappa, e} = 1$.

Remark 3.5. We remark that Definition 3.4 is one of the possible definitions of a local operator with the property of preserving a.e. constant functions for which Lemma 3.1 holds true. In the following analysis we just use the existence of such operator and the computation of the error estimator does not require any evaluation of such operator. In the proof of Lemma 3.1 we have used the continuity of the local operator \mathcal{S}_h^ω , its stability constant does not appear explicitly in the proof of (3.7). Nevertheless, the constants appearing in Lemma 3.1 can depend on this stability constant that can be relevant for example in an adaptive algorithm based on the derived a posteriori error estimates. For this reason we discuss the stability of the operator and its relation with the choice of the patches in the Appendix.

Remark 3.6. In the definition of I_h given in Ref. 34, under a quasi-monotonicity condition for the distribution of coefficients κ , we can resort to a modified Clément quasi interpolator as in Ref. 41, 19, 38 in case of discontinuous diffusivity coefficient in order to bound the constants $C_{\kappa,E}$ and $C_{\kappa,e}$.

3.2.2. A posteriori upper bound

The following result states the Galerkin orthogonality for those functions which are the image of a $H_0^1(\Omega)$ function through the operator P_h defined by Definition 3.4.

Lemma 3.2. *Let u_h be the solution to (2.6), u_h^π be defined by (3.1), $f \in L^2(\Omega)$ be the forcing term in (2.1), $f_h = \Pi_k^0 f$, κ the diffusivity coefficient, piecewise constant on the elements of \mathcal{T}_h , and P_h the operator defined by Definition 3.4. Then we have*

$$\sum_{E \in \mathcal{T}_h} a^E(u_h^\pi, P_h w) = (f_h, P_h w) \quad \forall w \in H_0^1(\Omega). \quad (3.14)$$

Proof. Since κ is constant on each element and $\nabla u_h^\pi \in [\mathbb{P}_{k-1}(\mathcal{T}_h)]^2$, we have that $(\kappa \nabla u_h^\pi, \nabla(P_h w))_E = (\kappa \nabla u_h^\pi, \Pi_{k-1}^0 \nabla(P_h w))_E \quad \forall E \in \mathcal{T}_h$. Then, using the VEM discrete variational formulation (2.6), the definition of u_h^π in (3.1) and the definition of P_h we obtain

$$\begin{aligned} \sum_{E \in \mathcal{T}_h} a^E(u_h^\pi, P_h w) &= \sum_{E \in \mathcal{T}_h} (\kappa \nabla u_h^\pi, \nabla(P_h w))_E = \sum_{E \in \mathcal{T}_h} (\kappa \nabla u_h^\pi, \Pi_{k-1}^0 \nabla(P_h w))_E = \\ &= \sum_{E \in \mathcal{T}_h} (\kappa \Pi_{k-1}^0 \nabla u_h, \Pi_{k-1}^0 \nabla(P_h w))_E = \sum_{E \in \mathcal{T}_h} (\kappa \Pi_{k-1}^0 \nabla u_h, \Pi_{k-1}^0 \nabla(P_h w))_E + \\ &\quad + S^E((I - \Pi_k^\nabla) u_h, (I - \Pi_k^\nabla) P_h w) = a_h(u_h, P_h w) = (f_h, P_h w). \quad \square \end{aligned}$$

Remark 3.7. If we admit a non-constant diffusivity on each polygon, we have that, on any given $E \in \mathcal{T}_h$,

$$\begin{aligned} (\kappa \nabla u_h^\pi, \nabla(P_h w))_E &= (\kappa \nabla u_h^\pi, \Pi_{k-1}^0 \nabla(P_h w))_E \\ &\quad + (\kappa \nabla u_h^\pi, \nabla(P_h w) - \Pi_{k-1}^0 \nabla(P_h w))_E, \end{aligned}$$

12

and it follows that

$$\begin{aligned}
 \sum_{E \in \mathcal{T}_h} a^E(u_h^\pi, P_h w) &= (f_h, P_h w) + (\kappa \nabla u_h^\pi, \nabla(P_h w) - \Pi_{k-1}^0 \nabla(P_h w))_E \leq (f_h, P_h w) \\
 &\quad + \sum_{E \in \mathcal{T}_h} \|\kappa \nabla u_h^\pi\|_E \|\nabla(P_h w) - \Pi_{k-1}^0 \nabla(P_h w)\|_E \leq (f_h, P_h w) \\
 &\quad + \sum_{E \in \mathcal{T}_h} h_E \|\kappa \nabla u_h^\pi\|_E \|\nabla(P_h w)\|_E \leq (f_h, P_h w) + \sum_{E \in \mathcal{T}_h} h_E \|\kappa \nabla u_h^\pi\|_E \|\nabla w\|_E .
 \end{aligned}$$

If we do not assume κ to be piecewise constant on the polygons of \mathcal{T}_h other terms appear in the estimates.

In the proof of the following major result, we will use the following estimate (Ref. 10 and (3.10)):

$$\forall E \in \mathcal{T}_h, \forall w \in \mathbf{H}^1(E), \|w - \Pi_k^0 w\|_E \lesssim \frac{h_E}{\sqrt{\kappa_E}} \|\sqrt{\kappa} \nabla w\|_E . \quad (3.15)$$

Definition 3.7. For any internal edge $e \in \mathcal{E}_h$ let us define a unit normal vector \mathbf{n}_e as the outward unit normal vector for the element on the right of e ($\mathbf{n}_e = \mathbf{n}_R$) and the jump of the co-normal derivative of u_h^π

$$\llbracket \kappa \nabla u_h^\pi \cdot \mathbf{n}_e \rrbracket_e = \kappa_R \nabla u_h^\pi|_R \cdot \mathbf{n}_R + \kappa_L \nabla u_h^\pi|_L \cdot \mathbf{n}_L = \kappa_R \nabla u_h^\pi|_R \cdot \mathbf{n}_e - \kappa_L \nabla u_h^\pi|_L \cdot \mathbf{n}_e .$$

Theorem 3.2. Let u be the solution to (2.2), u_h^π be defined by (3.1), and $f_h = \Pi_k^0 f$. Then,

$$\begin{aligned}
 \|u - u_h^\pi\| \lesssim &\left\{ C_\kappa^2 \left[\sum_{E \in \mathcal{T}_h} \frac{h_E^2}{\kappa_E} \|f_h + \nabla \cdot (\kappa \nabla u_h^\pi)\|_E^2 \right. \right. \\
 &\left. \left. + \sum_{e \in \mathcal{E}_h} \frac{h_e}{\kappa_e} \|\llbracket \kappa \nabla u_h^\pi \cdot \mathbf{n}_e \rrbracket_e\|_e^2 \right] + \sum_{E \in \mathcal{T}_h} \frac{h_E^2}{\kappa_E} \|f - f_h\|_E^2 \right\}^{\frac{1}{2}} ,
 \end{aligned}$$

being C_κ a constant depending on the constants in Lemma 3.1.

Proof. Let P_h be the operator defined by Definition 3.4. Let $w \in \mathbf{H}_0^1(\Omega)$. Using (3.14), the problem (2.2), the fact that $(f_h, \Pi_k^0 w) = (\Pi_k^0 f, \Pi_k^0 w) = (f, \Pi_k^0 w)$ and Green's formula, we have

$$\begin{aligned}
 \sum_{E \in \mathcal{T}_h} a^E(u - u_h^\pi, w) &= (f, w)_E - \sum_{E \in \mathcal{T}_h} (\kappa \nabla u_h^\pi, \nabla w)_E = (f_h, w)_E \\
 &\quad - \sum_{E \in \mathcal{T}_h} (\kappa \nabla u_h^\pi, \nabla w)_E + (f - f_h, w)_E = (f_h, w - P_h w)_E \\
 &\quad - \sum_{E \in \mathcal{T}_h} (\kappa \nabla u_h^\pi, \nabla(w - P_h w))_E + (f - f_h, w - \Pi_k^0 w)_E ,
 \end{aligned}$$

then, by Green's formula, the Cauchy-Schwarz inequality and by estimates (3.10), (3.11) and (3.15),

$$\begin{aligned}
\sum_{E \in \mathcal{T}_h} a^E(u - u_h^\pi, w) &= \sum_{E \in \mathcal{T}_h} (f_h + \nabla \cdot (\kappa \nabla u_h^\pi), w - P_h w)_E \\
&\quad - \sum_{e \in \mathcal{E}_h} (\llbracket \kappa \nabla u_h^\pi \cdot \mathbf{n}_e \rrbracket_e, w - P_h w)_e + (f - f_h, w - \Pi_k^0 w) \\
&\leq \sum_{E \in \mathcal{T}_h} \|f + \nabla \cdot (\kappa \nabla u_h^\pi)\|_E \|w - P_h w\|_E + \sum_{e \in \mathcal{E}_h} \|\llbracket \kappa \nabla u_h^\pi \cdot \mathbf{n}_e \rrbracket_e\|_e \|w - P_h w\|_e \\
&+ \sum_{E \in \mathcal{T}_h} \|f - f_h\|_E \|w - \Pi_k^0 w\|_E \lesssim \sum_{E \in \mathcal{T}_h} C_{\kappa, E} \frac{h_E}{\sqrt{\kappa_E}} \|f + \nabla \cdot (\kappa \nabla u_h^\pi)\|_E \|\sqrt{\kappa} \nabla w\|_{\tilde{\omega}_E} \\
&\quad + \sum_{e \in \mathcal{E}_h} C_{\kappa, e} \frac{h_e^{\frac{1}{2}}}{\sqrt{\kappa_e}} \|\llbracket \kappa \nabla u_h^\pi \cdot \mathbf{n}_e \rrbracket_e\|_e \|\sqrt{\kappa} \nabla w\|_{\tilde{\omega}_e} + \sum_{E \in \mathcal{T}_h} \frac{h_E}{\sqrt{\kappa_E}} \|f - f_h\|_E \|\sqrt{\kappa} \nabla w\|_E.
\end{aligned}$$

Finally, we obtain

$$\begin{aligned}
\sum_{E \in \mathcal{T}_h} a^E(u - u_h^\pi, w) &\lesssim \left\{ C_\kappa^2 \left[\sum_{E \in \mathcal{T}_h} \frac{h_E^2}{\kappa_E} \|f + \nabla \cdot (\kappa \nabla u_h^\pi)\|_E^2 \right. \right. \\
&\quad \left. \left. + \sum_{e \in \mathcal{E}_h} \frac{h_e}{\kappa_e} \|\llbracket \kappa \nabla u_h^\pi \cdot \mathbf{n}_e \rrbracket_e\|_e^2 \right] + \sum_{E \in \mathcal{T}_h} \frac{h_E^2}{\kappa_E} \|f - f_h\|_E^2 \right\}^{\frac{1}{2}} \|\sqrt{\kappa} \nabla w\|,
\end{aligned}$$

where C_κ depends on $\max\{\max_{E \in \mathcal{T}_h} C_{\kappa, E}, \max_{e \in \mathcal{E}_h} C_{\kappa, e}\}$ and the maximum number of elements in each patch. The thesis is obtained by the definition of the $\|\cdot\|$ -norm in (3.2). \square

4. Efficiency of the a posteriori estimate

This section is devoted to obtain lower bounds for the error measured in terms of the following error estimator:

$$\eta_R := \left\{ \sum_{E \in \mathcal{T}_h} \eta_{R, E}^2 \right\}^{\frac{1}{2}}, \quad (4.1)$$

where, for all $E \in \mathcal{T}_h$, we define

$$\eta_{R, E}^2 := \frac{h_E^2}{\kappa_E} \|f_h + \nabla \cdot (\kappa \nabla u_h^\pi)\|_E^2 + \frac{1}{2} \sum_{e \in \mathcal{E}_h \cap \partial E} \frac{h_e}{\kappa_e} \|\llbracket \kappa \nabla u_h^\pi \cdot \mathbf{n}_e \rrbracket_e\|_e^2. \quad (4.2)$$

4.1. Auxiliary results

The aim of this subsection is to extend the techniques based on triangle-bubble functions used in Ref. 46 to general polygons.

Consider a polygon $E \in \mathcal{T}_h$ and a triangle $t \in \mathcal{T}_{h,E}$. Let $\lambda_{t,i}$, $i = 1, 2, 3$, be the barycentric coordinates of t . Define the *triangle-bubble function* of t , $\mathbf{b}_t \in \mathbb{H}_0^1(t)$, as the function with support on t whose expression on t is $\mathbf{b}_t|_t := 27\lambda_{t,1}\lambda_{t,2}\lambda_{t,3}$. Using the above definition we can define the *polygon-bubble function* $\mathbf{b}_E \in \mathbb{H}_0^1(E)$ as the function with support on E such that $\mathbf{b}_E|_t := \mathbf{b}_t \forall t \in \mathcal{T}_{h,E}$. Note that $\mathbf{b}_E|_{\partial t} = 0 \forall t \in \mathcal{T}_{h,E}$. Next, consider an edge $e \in \mathcal{E}_h$ and define the *edge bubble-function* of e , $\mathbf{b}_e \in \mathbb{H}_0^1(\omega_e)$, as the function with support on ω_e and such that $\mathbf{b}_e|_r := 4\lambda_{r,1}\lambda_{r,2} \forall r \in \omega_e$, if we enumerate the vertices of r such that the vertices of e are numbered first. The following useful properties of the polygon-bubble functions follow from the classic estimates in Ref. 45 (Lemma 4.1) combined with (2.3).

Lemma 4.1. *Let $E \in \mathcal{T}_h$ and \mathbf{b}_E be the polygon-bubble function of E . Let $\mathcal{P}(E)$ be a polynomial space defined on E . Then, for any $v \in \mathcal{P}(E)$,*

$$\|v\|_E^2 \lesssim (v, v\mathbf{b}_E)_E, \quad \|\mathbf{b}_E v\|_E \leq \|v\|_E, \quad (4.3)$$

$$\|\nabla(\mathbf{b}_E v)\|_E \lesssim h_E^{-1} \|v\|_E. \quad (4.4)$$

Proof. Result (4.3) immediately follows from the fact that

$$\|v\|_t^2 \lesssim (v, v\mathbf{b}_t)_t, \quad \|\mathbf{b}_t v\|_t \leq \|v\|_E \quad \forall t \in \mathcal{T}_{h,E}$$

where the inequality constants are independent of any scale parameter of t (see Ref. 46). Regarding (4.4), classical results guarantee the fulfillment of the inequality on each $t \in \mathcal{T}_{h,E}$, i.e. $\forall E \in \mathcal{T}_h, \forall t \in \mathcal{T}_{h,E}, \|\nabla(\mathbf{b}_E v)\|_t = \|\nabla(\mathbf{b}_t v)\|_t \lesssim Ch_t^{-1} \|v\|_t$. Using (2.3), that implies $h_t \sim h_E$, we get $\|\nabla(\mathbf{b}_E v)\|_E \lesssim h_E^{-1} \|v\|_E$, with an equivalence constant depending on γ . \square

In order to state some useful properties of the edge-bubble functions, we first recall the concept of continuation of a function⁴⁶ from an edge to a triangle.

Definition 4.1 (Continuation operator). Let t be a triangle, σ one of its edges and $v \in C^\infty(\sigma)$. Let \hat{t} be the unitary triangle and let F be the mapping from \hat{t} to t such that $F([0, 1] \times \{0\}) = \sigma$. Let $\mathcal{C}_{\hat{t}}: C^\infty([0, 1] \times \{0\}) \rightarrow C^\infty(\hat{t})$ be the reference continuation operator, such that

$$\forall \hat{v} \in C^\infty([0, 1] \times \{0\}), \quad \mathcal{C}_{\hat{t}}(\hat{v})(\hat{x}, \hat{y}) = \hat{v}(\hat{x}, 0) \quad \forall (\hat{x}, \hat{y}) \in \hat{t}.$$

Then the *continuation* of v to t is $\mathcal{C}_t := \mathcal{C}_{\hat{t}} \circ F^{-1}$

Using classic estimates⁴⁶ and (2.3) we have the following properties for edge-bubble functions.

Lemma 4.2. *Let $e \in \mathcal{E}_h$ and \mathbf{b}_e be the edge-bubble function of e . Let $\mathcal{P}(e)$ be a*

polynomial space defined on e . Then, for any $v \in \mathcal{P}(e)$,

$$\begin{aligned} \|v\|_e^2 &\lesssim (v, v \mathbf{b}_e)_e, \\ \|\mathbf{b}_e v\|_e &\leq \|v\|_e, \\ \|\mathcal{C}_t(v) \mathbf{b}_e\|_t &\lesssim h_t^{\frac{3}{2}} \|v\|_e \quad \forall t \in \omega_e, \\ \|\nabla(\mathcal{C}_t(v) \mathbf{b}_e)\|_t &\lesssim h_t^{-\frac{1}{2}} \|v\|_e \quad \forall t \in \omega_e. \end{aligned} \quad (4.5)$$

Proof. The proof is analogous to the one of Lemma 4.1: classical results⁴⁶ give us the desired inequalities on sub-triangles, while (2.3) allows to extend them to the whole polygon with constants independent of the meshsize, but depending on the quality of the element.

In particular, regarding (4.5), we recall from Ref. 46 that, given the regularity assumptions and since \mathbf{b}_e is a positive function and $\max \mathbf{b}_e = 1$,

$$\forall t \in \omega_e, \|\mathbf{b}_e\|_t^2 = (\mathbf{b}_e, \mathbf{b}_e)_t \leq (\mathbf{b}_e, 1)_t = \frac{1}{3} |t| \sim h_e^2 \Rightarrow \|\mathbf{b}_e\|_{\omega_e} \lesssim h_e. \quad (4.6)$$

Let $V := \mathcal{C}_t(v)$. First of all, using (4.6), we see that

$$\|V \mathbf{b}_e\|_{\omega_e} \leq \|\mathbf{b}_e\|_{\omega_e} \|V\|_{\omega_e} \lesssim h_e \|V\|_{\omega_e} \leq h_e \sum_{t \in \omega_e} \|V\|_t. \quad (4.7)$$

Let $t \in \omega_e$. Indicating by \hat{t} the unitary triangle, by F the map from \hat{t} to t and setting $\hat{V} := V \circ F$,

$$\begin{aligned} \|V\|_t^2 &= \int_t V^2 = 2|t| \int_{\hat{t}} \hat{V}^2 = 2|t| \int_0^1 \int_0^{1-x} \hat{v}(\hat{x})^2 d\hat{y} d\hat{x} = \\ &= 2|t| \int_0^1 (1-\hat{x}) \hat{v}(\hat{x})^2 \leq 2|t| \int_0^1 \hat{v}(\hat{x})^2 = 2|t| h_e^{-1} \|v\|_e^2 \lesssim h_e \|v\|_e^2, \end{aligned}$$

where $\hat{v} := v \circ F = (V \circ F)|_{\hat{y}=0}$. It follows that $\|V\|_t \lesssim h_e^{\frac{1}{2}} \|v\|_e$ and, using (4.7), we obtain (4.5). \square

4.2. Lower bound

By standard techniques⁴⁶ and suitable global bubble functions^{21,22} we are able to prove the following lower bound.

Theorem 4.1. *Let u be the solution to (2.2), u_h^π be defined by (3.1), f be the right-hand side of (2.1), $f_h = \Pi_k^0 f$. Then, $\forall E \in \mathcal{T}_h$*

$$\eta_R \lesssim \left\{ \|u - u_h^\pi\|^2 + \sum_{E \in \mathcal{T}_h} \frac{h_E^2}{\kappa_E} \|f - f_h\|_E^2 \right\}^{\frac{1}{2}}, \quad (4.8)$$

where h is the maximum diameter of the discretization.

16

Proof. Let $E \in \mathcal{T}_h$ and let \mathfrak{b}_E be the bubble function of E . Let

$$w_E := \frac{h_E}{\sqrt{\kappa_E}} (f_h + \nabla \cdot (\kappa \nabla u_h^\pi)) \mathfrak{b}_E \in \mathbf{H}_0^1(E),$$

$$w := \sum_{E \in \mathcal{T}_h} w_E \in \mathbf{H}_0^1(\Omega).$$

Then, using Lemma 4.1, we prove that

$$\sqrt{\sum_{E \in \mathcal{T}_h} \frac{h_E^2}{\kappa_E} \|f_h + \nabla \cdot (\kappa \nabla u_h^\pi)\|_E^2} \lesssim \sqrt{\|u - u_h^\pi\|^2 + \sum_{E \in \mathcal{T}_h} \frac{h_E^2}{\kappa_E} \|f - f_h\|_E^2},$$

indeed,

$$\begin{aligned} & \sum_{E \in \mathcal{T}_h} \frac{h_E^2}{\kappa_E} \|f_h + \nabla \cdot (\kappa \nabla u_h^\pi)\|_E^2 \lesssim \sum_{E \in \mathcal{T}_h} \left(f_h + \nabla \cdot (\kappa \nabla u_h^\pi), \frac{h_E}{\sqrt{\kappa_E}} w_E \right)_E = \\ & = \sum_{E \in \mathcal{T}_h} \left(f, \frac{h_E}{\sqrt{\kappa_E}} w_E \right)_E - \left(\kappa \nabla u_h^\pi, \frac{h_E}{\sqrt{\kappa_E}} \nabla w_E \right)_E + \left(f_h - f, \frac{h_E}{\sqrt{\kappa_E}} w_E \right)_E = \\ & = \sum_{E \in \mathcal{T}_h} a^E \left(u - u_h^\pi, \frac{h_E}{\sqrt{\kappa_E}} w_E \right) + \sum_{E \in \mathcal{T}_h} \left(f_h - f, \frac{h_E}{\sqrt{\kappa_E}} w_E \right)_E \lesssim \\ & \lesssim \|u - u_h^\pi\| \sqrt{\sum_{E \in \mathcal{T}_h} \frac{h_E^2}{\kappa_E} \|\sqrt{\kappa} \nabla w\|_E^2} + \sum_{E \in \mathcal{T}_h} \frac{h_E}{\sqrt{\kappa_E}} \|f_h - f\|_E \|w_E\|_E \lesssim \\ & \lesssim \sqrt{\sum_{E \in \mathcal{T}_h} \|w\|_E^2} \left(\|u - u_h^\pi\|_E^2 + \frac{h_E^2}{\kappa_E} \|f - f_h\|_E^2 \right)^{\frac{1}{2}}. \end{aligned}$$

Now, consider an edge $e \in \mathcal{E}_h$ and let \mathfrak{b}_e be the edge-bubble function of e . Define $w_e \in \mathbf{H}_0^1(\omega_e)$ such that

$$w_e|_t := \mathcal{C}_t \left(\frac{\sqrt{h_e}}{\sqrt{\kappa_e}} \llbracket \kappa \nabla u_h^\pi \cdot \mathbf{n}_e \rrbracket_e \right) \mathfrak{b}_e \quad \forall t \subset \omega_e,$$

$$w := \sum_{e \in \mathcal{E}_h} w_e \in \mathbf{H}_0^1(\Omega).$$

From Lemma 4.2 and regularity assumptions on the elements $E \in \mathcal{T}_h$ it follows that

$$\sqrt{\sum_{e \in \mathcal{E}_h} \frac{h_e}{\kappa_e} \|\llbracket \kappa \nabla u_h^\pi \cdot \mathbf{n}_e \rrbracket_e\|_e^2} \lesssim \sqrt{(1 + h^2) \|u - u_h^\pi\|^2 + \sum_{E \in \mathcal{T}_h} \frac{h_E^4}{\kappa_E} \|f - f_h\|_E^2},$$

indeed,

$$\begin{aligned}
& \sum_{e \in \mathcal{E}_h} \frac{h_e}{\kappa_e} \|\llbracket \kappa \nabla u_h^\pi \cdot \mathbf{n}_e \rrbracket_e\|_e^2 \lesssim \sum_{e \in \mathcal{E}_h} \left(\llbracket \kappa \nabla u_h^\pi \cdot \mathbf{n}_e \rrbracket_e, \sqrt{\frac{h_e}{\kappa_e}} w_e \right)_e = \\
& = \sum_{e \in \mathcal{E}_h} \sum_{t \in \omega_e} \left(\kappa \nabla u_h^\pi, \sqrt{\frac{h_e}{\kappa_e}} \nabla w_e \right)_t + \left(\nabla \cdot (\kappa \nabla u_h^\pi), \sqrt{\frac{h_e}{\kappa_e}} w_e \right)_t \\
& = \sum_{E \in \mathcal{T}_h} a^E \left(u_h^\pi - u, \sum_{e \in \mathcal{E}_h} \sqrt{\frac{h_e}{\kappa_e}} w_e \right) + \sum_{e \in \mathcal{E}_h} \sum_{t \in \omega_e} \left(f + \nabla \cdot (\kappa \nabla u_h^\pi), \sqrt{\frac{h_e}{\kappa_e}} w_e \right)_t \\
& \lesssim \|u - u_h^\pi\| \sqrt{\sum_{e \in \mathcal{E}_h} \frac{h_e}{\kappa_e} \|\sqrt{\kappa} \nabla w_e\|_{\omega_e}^2} + \sum_{e \in \mathcal{E}_h} \sum_{t \in \omega_e} \sqrt{\frac{h_e}{\kappa_e}} \|(f + \nabla \cdot (\kappa \nabla u_h^\pi))\|_t \|w_e\|_t \lesssim \\
& \lesssim \left(\|u - u_h^\pi\|^2 + \sum_{E \in \mathcal{T}_h} \left(\frac{h_E^4}{\kappa_E} \|f - f_h\|_E^2 + \frac{h_E^4}{\kappa_E} \|f_h + \nabla \cdot (\kappa \nabla u_h^\pi)\|_E^2 \right) \right)^{\frac{1}{2}} \times \\
& \times \sqrt{\sum_{e \in \mathcal{E}_h} \frac{h_e}{\kappa_e} \|\llbracket \kappa \nabla u_h^\pi \cdot \mathbf{n}_e \rrbracket_e\|_e^2} \lesssim \sqrt{\sum_{e \in \mathcal{E}_h} \frac{h_e}{\kappa_e} \|\llbracket \kappa \nabla u_h^\pi \cdot \mathbf{n}_e \rrbracket_e\|_e^2} \left((1 + h^2) \|u - u_h^\pi\|^2 \right. \\
& \left. + \sum_{E \in \mathcal{T}_h} \frac{h_E^4}{\kappa_E} \|f - f_h\|_E^2 \right)^{\frac{1}{2}}.
\end{aligned}$$

Recalling the definition of η_R , given by (4.1), and neglecting higher order terms, the thesis follows. \square

5. Numerical results

In the following we present some numerical tests performed in order to numerically evaluate the *effectivity index*, defined as

$$\epsilon := \frac{err}{\eta_R} \quad \text{where} \quad err := \left\{ \sum_{E \in \mathcal{T}_h} \|\sqrt{\kappa} \nabla (u - u_h^\pi)\|_E^2 \right\}^{\frac{1}{2}}. \quad (5.1)$$

A constant behaviour of the effectivity index shows that the constants of equivalence between exact and estimated error are independent of the meshsize, element distortion and diffusivity jumps. Several VEM orders are considered.

In order to test the behaviour of the effectivity index we first perform several tests on the simple domain $\Omega = [0, 1] \times [0, 1]$, as shown in Figure 1, possibly split in subregions (Figure 1a-1c: 1 subdomain, Figure 1d: 2 subdomains, Figure 1e: 4 subdomains) with different diffusivity coefficients on each subdomain. Several meshes are considered to test the behaviour of the estimators on a quasi-uniform mesh (Figures 1a and 1b), as well as on a highly distorted Voronoi mesh (Figure 1c).

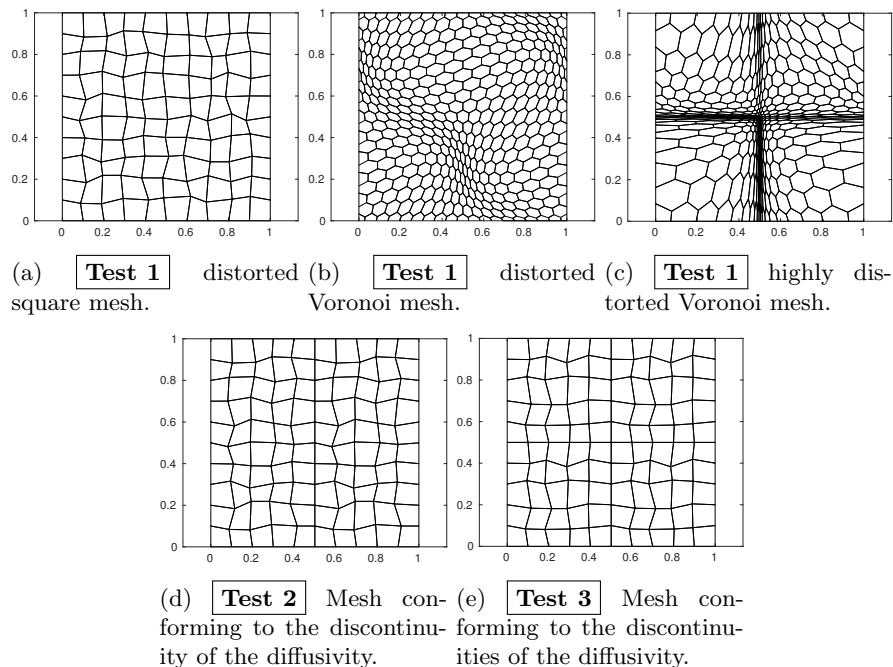


Figure 1: Meshes used.

 Table 1: **Test 1** Convergence rates.

Mesh	$k = 1$		$k = 2$		$k = 3$		$k = 4$	
	err	η_R	err	η_R	err	η_R	err	η_R
Figure 1a	1.0228	1.0275	2.0581	2.0578	3.0790	3.0777	4.1177	4.1149
Figure 1b	0.9876	0.9983	1.9707	1.9688	2.9784	2.9848	3.9772	3.9658
Figure 1c	1.0667	1.1105	2.0860	1.9827	3.2413	3.2719	-	-

5.1. Test 1: Robustness with respect to mesh distortion

We consider a constant diffusivity $\kappa(x, y) = 1$ and we set the loading term f in such a way that the solution of the problem is $u(x, y) = \sin(2\pi x) \sin(2\pi y)$. We are interested in testing the independence of the effectivity index of the meshsize and in observing its variation with respect to different mesh shapes. First, we consider two families of good quality meshes made up of mildly distorted squares and Voronoi polygons⁴⁴ (Figures 1a and 1b). In Figures 2 and 3 we compare the exact error err defined by (5.1) and the error estimator η_R defined by (4.1). We see that the two quantities have the same rate of convergence (see also Table 1). This agreement is confirmed by Tables 2 and 3, which show that the effectivity indices are essentially

independent of the meshsize. Moreover, comparing the two tables we see that the effectivity indices corresponding to the same VEM order are quite comparable, thus showing that the efficiency of the estimate is not affected by the type of polygons we choose to discretize the domain.

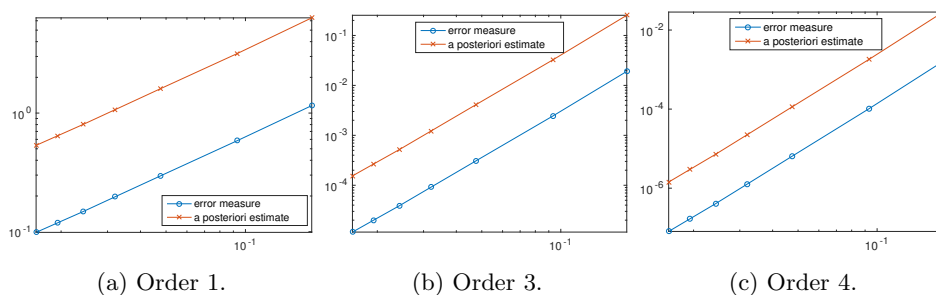


Figure 2: **Test 1, distorted square mesh** Error measure and error estimator vs. maximum diameter of the discretization.

Table 2: **Test 1, distorted square mesh** Effectivity indices.

$k = 1$		$k = 2$		$k = 3$		$k = 4$	
h	ϵ	h	ϵ	h	ϵ	h	ϵ
0.1784	0.1821	0.1784	0.1106	0.1784	0.0752	0.1784	0.0567
0.0933	0.1843	0.0933	0.1104	0.0933	0.0752	0.0933	0.0566
0.0475	0.1841	0.0475	0.1106	0.0475	0.0749	0.0475	0.0565
0.0321	0.1844	0.0321	0.1106	0.0321	0.0751	0.0321	0.0563
0.0243	0.1843	0.0243	0.1106	0.0243	0.0750	0.0243	0.0563
0.0194	0.1846	0.0194	0.1105	0.0194	0.0750	0.0194	0.0563
0.0161	0.1847	0.0161	0.1105	0.0161	0.0750	0.0161	0.0563

To test the robustness of the estimate in presence of bad quality polygons, we solve the same problem on the mesh in Figure 1c, using VEM of order 1 to 3. We do not use larger values for the VEM order as the resulting linear systems turn out to be too badly assembled due to the ill conditioning of the local projection matrices.²⁴ From Figure 4 we see the good agreement between the exact error and the a posteriori estimate (see also Table 1 for the computed convergence rates). These results are confirmed by Table 4, from which we can observe that the effectivity index is not significantly affected by the presence of oddly shaped polygons. In particular, the effectivity indices do not depend significantly on the meshsize, mesh distortion, and they are comparable to the ones corresponding to the same

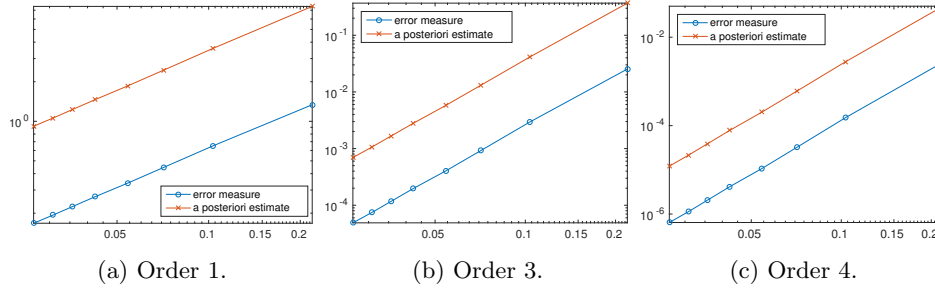


Figure 3: **Test 1, distorted Voronoi mesh** Error measure and error estimator vs. maximum diameter of the discretization.

Table 3: **Test 1, distorted Voronoi mesh** Effectivity indices.

$k = 1$		$k = 2$		$k = 3$		$k = 4$	
h	ϵ	h	ϵ	h	ϵ	h	ϵ
0.2190	0.1786	0.2190	0.1005	0.2190	0.0687	0.2190	0.0539
0.1033	0.1814	0.1033	0.1026	0.1033	0.0712	0.1033	0.0544
0.0711	0.1820	0.0711	0.1012	0.0711	0.0703	0.0711	0.0535
0.0542	0.1822	0.0542	0.1004	0.0542	0.0698	0.0542	0.0530
0.0423	0.1827	0.0423	0.1013	0.0423	0.0706	0.0423	0.0534
0.0357	0.1827	0.0357	0.1008	0.0357	0.0702	0.0357	0.0530
0.0308	0.1827	0.0308	0.1004	0.0308	0.0700	0.0308	0.0528
0.0266	0.1830	0.0266	0.1010	0.0266	0.0704	0.0266	0.0531

order k computed on the previous two meshes (Tables 2 and 3). The dependence on the mesh regularity parameter is more evident from the effectivity indices shown in Table 5, which are computed only on the elements belonging to the two central horizontal and vertical bands $\omega_{vd} = (0.475, 0.525) \times (0, 1) \cup (0, 1) \times (0.475, 0.525)$, where very distorted elements do concentrate. We see that the effectivity indices are still asymptotically constant, but comparing the values in Tables 4 and 5 we can find that their values are influenced by the distortion of the elements.

5.2. Test 2: Robustness with respect to diffusivity jumps

We consider here two further tests featuring discontinuous piecewise constant diffusivities $\kappa_1(x, y)$ and $\kappa_2(x, y)$ satisfying a quasi-monotonicity condition (see Remark 3.6) defined on $\Omega = [0, 1] \times [0, 1]$ as follows:

$$\kappa_1(x, y) := \begin{cases} 10 & \text{in } \Omega_1 = [0, 0.5] \times [0, 1], \\ 1 & \text{in } \Omega_2 = (0.5, 1] \times [0, 1]. \end{cases}$$

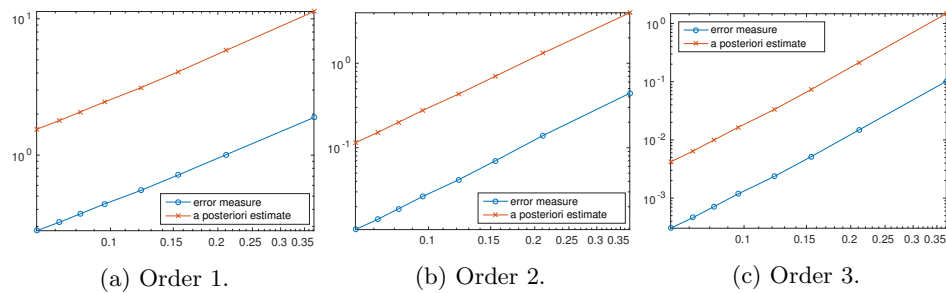


Figure 4: **Test 1, highly distorted Voronoi mesh** Error measure and error estimator vs. maximum diameter of the discretization.

Table 4: **Test 1, highly distorted Voronoi mesh** Effectivity indices.

$k = 1$		$k = 2$		$k = 3$	
h	ϵ	h	ϵ	h	ϵ
0.3720	0.1668	0.3720	0.1115	0.3720	0.0688
0.2111	0.1718	0.2111	0.1058	0.2111	0.0695
0.1547	0.1748	0.1547	0.0996	0.1547	0.0702
0.1217	0.1765	0.1217	0.0967	0.1217	0.0708
0.0962	0.1785	0.0962	0.0958	0.0962	0.0717
0.0822	0.1790	0.0822	0.0946	0.0822	0.0719
0.0718	0.1795	0.0718	0.0937	0.0718	0.0721
0.0621	0.1803	0.0621	0.0936	0.0621	0.0724

Table 5: **Test 1, highly distorted Voronoi mesh** Effectivity indices computed on highly distorted polygons only.

$k = 1$		$k = 2$		$k = 3$	
h	ϵ	h	ϵ	h	ϵ
0.3720	0.6171	0.3720	0.3150	0.3720	0.1602
0.2111	0.3445	0.2111	0.3280	0.2111	0.1859
0.1547	0.3009	0.1547	0.2984	0.1547	0.2049
0.1217	0.2825	0.1217	0.2787	0.1217	0.2156
0.0962	0.2847	0.0962	0.2781	0.0962	0.2295
0.0822	0.2774	0.0822	0.2697	0.0822	0.2363
0.0718	0.2714	0.0718	0.2643	0.0718	0.2371
0.0621	0.2727	0.0621	0.2664	0.0621	0.2412

10	1	10 ⁻³	1	10 ⁻²	10	10 ⁻²	10 ⁵
1	10 ⁻³	1	10 ⁻³	1	10 ⁻³	1	10 ⁻⁷
(a) κ_1		(b) κ_2		(c) κ_3		(d) κ_4	

Figure 5: **Test 2**: subfigures a and b, **Test 3**: subfigures c and d; distributions of diffusivity coefficients considered in Sec. 5.2 and 5.3, respectively.

$$\kappa_2(x, y) := \begin{cases} 10^{-3} & \text{in } \Omega_1 = [0, 0.5] \times [0, 1], \\ 1 & \text{in } \Omega_2 = (0.5, 1] \times [0, 1]. \end{cases}$$

See Figures 5a and 5b for a representation of these coefficients. In both cases, the loading term is chosen in such a way that the solution corresponding to $\kappa_i(x, y)$ is $u_i(x, y) = \xi_i(x)Y(y)$, where

$$\xi_i(x) := \begin{cases} -\frac{1}{\kappa_i|_{\Omega_1}} \left(\frac{x^2}{2} + c_i x \right) & \text{if } x \in [0, \frac{1}{2}], \\ -\frac{1}{\kappa_i|_{\Omega_2}} \left(\frac{x^2}{2} + c_i x - c_i - \frac{1}{2} \right) & \text{if } x \in (\frac{1}{2}, 1], \end{cases} \quad (5.2)$$

$$Y(y) := y(1-y) \left(y - \frac{1}{2} \right)^2, \quad (5.3)$$

and $c_i := -\frac{3\kappa_i|_{\Omega_1} + \kappa_i|_{\Omega_2}}{4(\kappa_i|_{\Omega_1} + \kappa_i|_{\Omega_2})}$ is chosen in such a way that $-\kappa_i \frac{d^2 \xi_i}{dx^2} = 1$. In Figure 6a we show the solution u_1 . We used Virtual Elements of order 1 to 4 with meshes made up of deformed squares conforming to the discontinuity (central vertical line), as in Figure 1d. To compare the error estimate and the exact error, we show in Table 6 the rates of convergence computed from the tests performed, which are optimal. Tables 7 and 8 contain the computed effectivity indices. These are stable with respect to the meshsize and we observe that their values are comparable to the ones obtained for the other cases with the same VEM order. Moreover, we notice a very weak dependence of the effectivity indices on the jump of the diffusivity coefficient denoting a good robustness with respect to this property.

Remark 5.1. In the definition of the projection operator P_h provided in Subsection 3.2.1 we do not consider any particular strategy to contain the jumps of the diffusivity coefficients within the patches ω_E , and consequently the constants $C_{\kappa, E}$. In this example, the diffusivity distribution satisfies the *quasi-monotonicity* condition and consequently the definition of the Clément quasi-interpolator used in the definition of the operator I_h (Definition 3.3 and Ref. 34) can be replaced by the modified versions in Ref. 41, 19, 38 leading to robust estimates (3.10) and (3.11).

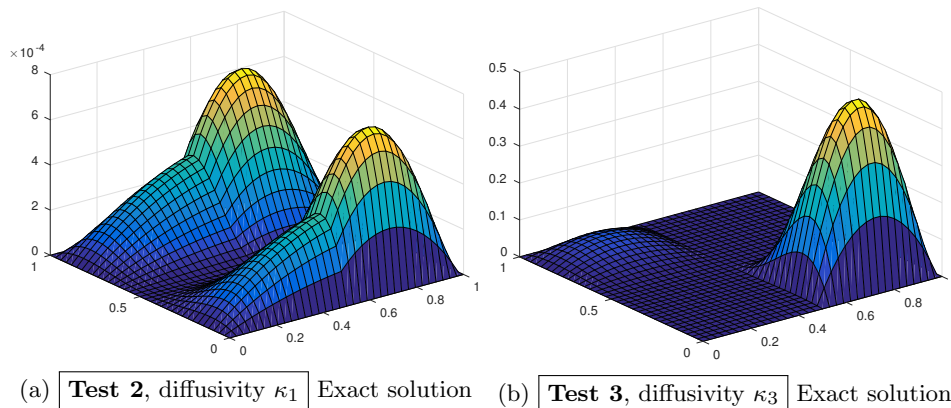


Figure 6: Two solutions with diffusivity jumps

 Table 6: **Test 2** Convergence rates.

	$k = 1$		$k = 2$		$k = 3$		$k = 4$	
Diffusivity	err	η_R	err	η_R	err	η_R	err	η_R
κ_1	1.0567	1.0076	2.0792	2.0700	3.0811	3.0666	4.1207	4.1128
κ_2	1.0433	1.0112	2.0463	2.0378	3.0579	3.0466	4.1165	4.1077

 Table 7: **Test 2**, diffusivity κ_1 Effectivity indices.

$k = 1$		$k = 2$		$k = 3$		$k = 4$	
h	ϵ	h	ϵ	h	ϵ	h	ϵ
0.1784	0.1821	0.1784	0.1291	0.1784	0.1113	0.1784	0.0873
0.1449	0.2281	0.1449	0.1403	0.1449	0.1173	0.1449	0.0891
0.0741	0.2272	0.0741	0.1401	0.0741	0.1152	0.0741	0.0881
0.0379	0.2263	0.0379	0.1412	0.0379	0.1156	0.0379	0.0885
0.0194	0.1805	0.0194	0.1312	0.0194	0.1097	0.0194	0.0860
0.0097	0.1801	0.0097	0.1312	0.0097	0.1099		
0.0049	0.1798						

5.3. Test 3: Checkerboard discontinuous diffusivity

A further test is performed in order to investigate problems without quasi-

Table 8: **Test 2**, diffusivity κ_2 Effectivity indices.

$k = 1$		$k = 2$		$k = 3$		$k = 4$	
h	ϵ	h	ϵ	h	ϵ	h	ϵ
0.1784	0.1825	0.1784	0.1630	0.1784	0.1290	0.1784	0.0925
0.1449	0.2135	0.1449	0.1729	0.1449	0.1285	0.1449	0.0931
0.0741	0.2121	0.0741	0.1712	0.0741	0.1257	0.0741	0.0918
0.0379	0.2119	0.0379	0.1733	0.0379	0.1254	0.0379	0.0921
0.0194	0.1823	0.0194	0.1639	0.0194	0.1250	0.0194	0.0908
0.0097	0.1820	0.0097	0.1638	0.0097	0.1248		
0.0049	0.1818						

Table 9: **Test 3** Convergence rates.

	$k = 1$		$k = 2$		$k = 3$		$k = 4$	
	err	η_R	err	η_R	err	η_R	err	η_R
κ_3	1.0032	1.0075	2.0211	2.0353	3.0351	3.0316	4.0757	4.0634
κ_4	1.0022	1.0075	2.0194	2.0345	3.0328	3.0292	4.0731	4.0594

monotone diffusivity coefficients⁴¹ (see Figure 5c and 5d):

$$\kappa_3(x, y) := \begin{cases} 1 & \text{in } \Omega_{11} = [0, 0.5]^2, \\ 10^{-3} & \text{in } \Omega_{12} = [0.5, 1] \times [0, 0.5), \\ 10^{-2} & \text{in } \Omega_{21} = [0, 0.5) \times [0.5, 1], \\ 10 & \text{in } \Omega_{22} = [0.5, 1]^2. \end{cases} \quad \kappa_4 := \begin{cases} 1 & \text{in } \Omega_{11}, \\ 10^{-7} & \text{in } \Omega_{12}, \\ 10^{-2} & \text{in } \Omega_{21}, \\ 10^5 & \text{in } \Omega_{22}. \end{cases}$$

This kind of distribution of the diffusivity coefficient are usually a limitation in deriving efficient a posteriori error estimators based on Clément type quasi-interpolation operators,⁴¹ nonetheless the numerical results which follow show that the estimates here derived are robust with respect to diffusivity jumps and distribution. The forcing terms are defined in such a way that the exact solutions are

$$u_i(x, y) := \begin{cases} \xi_i(x)Y(y) & \text{in } \Omega_{11} \cup \Omega_{21}, \\ \xi_i(1-x)Y(y) & \text{in } \Omega_{12} \cup \Omega_{22}, \end{cases}$$

$$\text{where } c_i := \begin{cases} -\frac{3\kappa_i|_{\Omega_{11}} + \kappa_i|_{\Omega_{12}}}{4(\kappa_i|_{\Omega_{11}} + \kappa_i|_{\Omega_{12}})} & \text{in } \Omega_{11} \cup \Omega_{12}, \\ -\frac{3\kappa_i|_{\Omega_{21}} + \kappa_i|_{\Omega_{22}}}{4(\kappa_i|_{\Omega_{21}} + \kappa_i|_{\Omega_{22}})} & \text{in } \Omega_{21} \cup \Omega_{22}, \end{cases} \quad i \in \{3, 4\}.$$

In Figure 6b we show the solution u_3 . As done for the test in Subsection 5.2, we show in Table 9 the computed convergence rates for the exact error err and the a posteriori estimate η_R , proving to be optimal. In addition, Tables 10 and 11 report the computed effectivity indices, which prove that the estimate is robust

even though the diffusivity lacks quasi-monotonicity condition. Again, the values of the effectivity indices are comparable to those obtained for the other tests for the same VEM order. Finally, we can see that the computed effectivity indices are not significantly affected by the jumps of κ , although the effectivity indices could be affected by these jumps by Lemma 3.1.

Table 10: **Test 3**, diffusivity κ_3 Effectivity indices.

$k = 1$		$k = 2$		$k = 3$		$k = 4$	
h	ϵ	h	ϵ	h	ϵ	h	ϵ
0.1799	0.1761	0.1799	0.1538	0.1799	0.1240	0.1799	0.0938
0.0892	0.1840	0.0892	0.1671	0.0892	0.1292	0.0892	0.0917
0.0466	0.1827	0.0466	0.1639	0.0466	0.1261	0.0466	0.0914
0.0238	0.1817	0.0238	0.1646	0.0238	0.1249	0.0238	0.0911
0.0190	0.1815	0.0190	0.1641	0.0190	0.1252	0.0190	0.0909
0.0097	0.1816	0.0097	0.1637	0.0097	0.1246		
0.0049	0.1819						

Table 11: **Test 3**, diffusivity κ_4 Effectivity indices.

$k = 1$		$k = 2$		$k = 3$		$k = 4$	
h	ϵ	h	ϵ	h	ϵ	h	ϵ
0.1799	0.1753	0.1799	0.1545	0.1799	0.1242	0.1799	0.0942
0.0892	0.1841	0.0892	0.1687	0.0892	0.1297	0.0892	0.0917
0.0466	0.1828	0.0466	0.1652	0.0466	0.1265	0.0466	0.0915
0.0238	0.1817	0.0238	0.1660	0.0238	0.1251	0.0238	0.0911
0.0190	0.1815	0.0190	0.1654	0.0190	0.1256	0.0190	0.0909
0.0097	0.1817	0.0097	0.1650	0.0097	0.1249		
0.0049	0.1820						

5.4. Test 4: irregular solution

Here we test the behaviour of the a posteriori estimate on a problem whose exact solution displays a bounded smoothness^{42,48}. Let

$$\kappa_5(x, y) := \begin{cases} 100 & \text{in } \Omega_{11} = [0, 0.5]^2, \\ 1 & \text{in } \Omega_{12} = [0.5, 1] \times [0, 0.5), \\ 1 & \text{in } \Omega_{21} = [0, 0.5) \times [0.5, 1], \\ 100 & \text{in } \Omega_{22} = [0.5, 1]^2. \end{cases}$$

Table 12: **Test 4** First choice for the coefficients

$\alpha = 1.873097930277786$		
Ω_{ij}	a_{ij}	b_{ij}
Ω_{11}	0.480354867169885	-0.882756592490932
Ω_{12}	-7.701564882495475	-6.456461752439308
Ω_{21}	9.603960396039620	2.960396039603962
Ω_{22}	-0.100000000000000	1.000000000000000

Table 13: **Test 4** Second choice for the coefficients

$\alpha = 0.126902069722214$		
Ω_{ij}	a_{ij}	b_{ij}
Ω_{11}	-0.480354867169885	-0.882756592490932
Ω_{12}	7.701564882495503	-6.456461752439336
Ω_{21}	-9.603960396039598	2.960396039603959
Ω_{22}	0.100000000000000	1.000000000000000

Table 14: **Test 4, First choice** Effectivity indices

$k = 1$		$k = 2$		$k = 3$	
h	ϵ	h	ϵ	h	ϵ
0.1976	0.4014	0.1976	0.1951	0.1976	0.1040
0.0699	0.3897	0.0699	0.1833	0.0699	0.0963
0.0217	0.3877	0.0217	0.1854	0.0217	0.0969
0.0071	0.3904	0.0071	0.1869	0.0159	0.0973

Let $u_5 : \Omega \rightarrow \mathbb{R}$ be the function whose expression in polar coordinates with center in $(\frac{1}{2}, \frac{1}{2})$ and with axes parallel to the standard axes is

$$u_5(\rho, \theta) := \rho^\alpha (a_{ij} \sin(\alpha\theta) + b_{ij} \cos(\alpha\theta)) .$$

This function non-trivially satisfies $-\nabla \cdot (\kappa_5 \nabla u_5) = 0$ for certain choices of the coefficients, in which cases it belongs to $H^{1+\alpha}(\Omega)$. We present here tests with the choices in Tables 12 and 13, done with VEM of order 1 to 3 on a triangular mesh conforming to the discontinuities of the diffusivity function. In Tables 14 and 15 we see how the effectivity indices are subject to bounded oscillations as we refine the mesh. Finally, in Table 16 we report the computed rates of convergence for both the choices of coefficients, we can notice a very good agreement with the expected theoretical values $\min\{k, \alpha\}$.

Table 15: **Test 4**, Second choice Effectivity indices

$k = 1$		$k = 2$		$k = 3$	
h	ϵ	h	ϵ	h	ϵ
0.1976	0.7870	0.1976	0.4221	0.1976	0.2208
0.0699	0.8493	0.0699	0.4380	0.0699	0.2270
0.0217	0.8604	0.0217	0.4341	0.0217	0.2244
0.0159	0.9176	0.0159	0.4654	0.0159	0.2368
0.0050	0.8832	0.0050	0.4391		

Table 16: **Test 4** Convergence rates.

	$k = 1$		$k = 2$		$k = 3$	
coefficients	err	η_R	err	η_R	err	η_R
Table 12	0.9991	0.9998	1.7641	1.7727	1.7443	1.7509
Table 13	0.1435	0.1475	0.1312	0.1233	0.1598	0.1778

5.5. Test DFN: A test on a Discrete Fracture Network

As a final, more general test, we consider a Discrete Fracture Network (DFN, Figure 7), that is a possible way to model an impervious fractured medium, consisting in a set of planar rectangles intersecting in space (see Ref. 1). In Ref. 18, the flexibility of the Virtual Element Method in handling hanging nodes as vertices of a polygon that correspond to a flat angle is used to obtain a mesh which is globally conforming to the intersections, allowing the application of domain decomposition techniques. On such domain, the hydraulic head distribution satisfies equation (2.1) on each rectangle, with coupling conditions given by the continuity of the solution and balance of incoming and outgoing fluxes at each intersection. The numerical tools developed in the present work can be easily applied to this framework, giving a slightly modified a posteriori error estimator:

$$\begin{aligned} \tilde{\eta}_{R,E}^2 := & \frac{h_E^2}{\kappa_E} \|f_h + \nabla \cdot (\kappa \nabla u_h^\pi)\|_E^2 + \frac{1}{2} \sum_{e \in \mathcal{E}_h^{\text{int}} \cap \partial E} \frac{h_e}{\kappa_e} \|[\kappa \nabla u_h^\pi \cdot \mathbf{n}_e]_e\|_e^2 \\ & + \frac{1}{4} \sum_{e \in \mathcal{E}_h^{\text{tr}} \cap \partial E} \frac{h_e}{\kappa_e} \|[\kappa \nabla u_{h_{i_e}}^\pi \cdot \mathbf{n}_e]_e + [\kappa \nabla u_{h_{j_e}}^\pi \cdot \mathbf{n}_e]_e\|_e^2, \end{aligned}$$

where $\mathcal{E}_h^{\text{tr}}$ is the set of edges which lie on some of the rectangle intersections, $\mathcal{E}_h^{\text{int}}$ the other internal edges of the fracture, and $u_{h_{i_e}}^\pi$ and $u_{h_{j_e}}^\pi$ are the restrictions of the projection of the discrete solution to the two fractures intersecting at e .

The geometry of the DFN we consider for the numerical tests is shown in Figure 7, the diffusivity coefficient is $\kappa(x, y) = 1$, more details on this test problem can be found in Ref. 15, Subsection 6.1. In Table 18 we show the effectivity indices

Table 17: **Test DFN** Convergence rates.

$k = 1$		$k = 2$	
err	η_R	err	η_R
1.0302	1.0341	2.0810	2.0813

computed on progressively refined grids for linear and quadratic VEM, whereas in Figure 8 the a posteriori estimate is compared to the error measure. The convergence rates of err and η_R are shown in Table 17 for $k = 1, 2$.

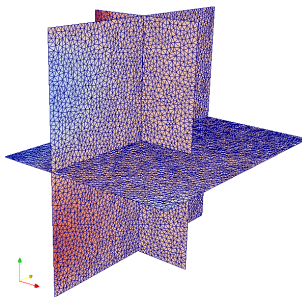


Figure 7: **Test DFN** The Discrete Fracture Network considered.

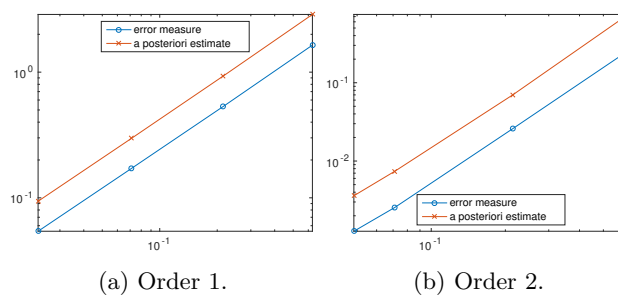


Figure 8: **Test DFN** Error measure and error estimator vs. maximum diameter of the discretization.

6. Conclusions

We have considered the issue of deriving an a posteriori error estimate for the Virtual Element Method formulation of a simple Poisson problem with discontinuous

Table 18: **Test DFN** Effectivity indices.

$k = 1$		$k = 2$	
h	ϵ	h	ϵ
0.6305	0.5699	0.6305	0.3438
0.2144	0.5725	0.2144	0.3702
0.0712	0.5764	0.0712	0.3449
0.0231	0.5770	0.0485	0.3522

viscosity coefficient completely independent of the particular choice of the VEM stabilization. The numerical solution obtained with a VEM discretization is usually provided through some degrees of freedom that do not allow an easy and direct evaluation of the solution on all the domain. We have introduced a suitable projection of the solution onto a piecewise polynomial space on each element, which can be used for solution evaluation and to define an error measure between such projection and the exact solution. An equivalence relation between the error and the analyzed error estimator can be provided avoiding terms related to the VEM stabilization in the error estimator. The analysis here developed is based on a stability assumption on the operator \mathcal{S}_h^ω addressed numerically in Appendix.

Numerical results clearly show a very good agreement between the error estimator and the exact error, with an almost constant effectivity index confirming that the constants involved in the equivalence relation are independent of the meshsize and the diffusivity jump distribution. In the numerical results we also naturally address a DFN flow problem introducing in the estimates the effect of the flux balance at the fracture intersections; again, an almost constant effectivity index is found.

The proposed approach to the a posteriori error analysis of the error of a polynomial approximation can be extended to more complex problems and is currently under investigation.

7. Appendix: stability of the operator \mathcal{S}_h^ω

In this section we provide a short discussion on the stability properties of the operator \mathcal{S}_h^ω .

Lemma 7.1. *Let $v_h \in V_h$, ω be a patch such that the degree of freedom r satisfies condition (4) in Definition 3.1. Let $\mathbf{w} = \frac{\mathbf{u}_h^\top (\mathbf{I} - \mathbf{\Pi}^\nabla)^\top (\mathbf{I} - \mathbf{\Pi}^\nabla)}{\|\mathbf{u}_h^\top (\mathbf{I} - \mathbf{\Pi}^\nabla)^\top (\mathbf{I} - \mathbf{\Pi}^\nabla)\|_\infty}$, where $\mathbf{\Pi}^\nabla \in \mathbb{R}^{N_\omega \times N_\omega}$ is the matrix representing the operator Π_k^∇ on the degrees of freedom of ω , N_ω is the total number of degrees of freedom in ω and \mathbf{u}_h is the vector of the degrees of freedom of the solution on ω , ordered in such a way that the last one is r . Then,*

$$\|\mathcal{S}_h^\omega v_h\| \lesssim \max \left\{ 1, \frac{1}{|w_{N_\omega}|} \right\} \|v_h\|. \quad (7.1)$$

Proof. Let $\mathbf{s}_v, \mathbf{v}_h$ be the vectors of degrees of freedom of $\mathcal{S}_h^\omega v_h$ and v_h , respectively, ordered in such a way that the last one is r . Then, condition (3.4) is equivalent to $\frac{\mathbf{w}}{w_{N_\omega}} \cdot \mathbf{s}_v = 0$. Then, \mathbf{s}_v is obtained from \mathbf{v}_h by

$$\mathbf{s}_v = \mathbf{M}^{-1} \begin{pmatrix} \tilde{\mathbf{v}}_h \\ 0 \end{pmatrix}, \quad (7.2)$$

where $\tilde{\mathbf{v}}_h \in \mathbb{R}^{N_\omega-1}$ is the vector of all the degrees of freedom of v_h except for the last one (corresponding to the index r in the original numbering), and

$$\mathbf{M} = \begin{pmatrix} \tilde{\mathbf{I}} & \mathbf{0} \\ -\frac{\tilde{\mathbf{w}}}{w_{N_\omega}} & 1 \end{pmatrix},$$

where $\tilde{\mathbf{I}} \in \mathbb{R}^{(N_\omega-1) \times (N_\omega-1)}$ is the identity matrix of order $N_\omega - 1$. From (7.2), we have

$$\|\mathbf{s}_v\|_{\mathbb{R}^{N_\omega}} \leq \|\mathbf{M}^{-1}\|_{\mathbb{R}^{N_\omega \times N_\omega}} \|\tilde{\mathbf{v}}_h\|_{\mathbb{R}^{N_\omega-1}} \leq \|\mathbf{M}^{-1}\|_{\mathbb{R}^{N_\omega \times N_\omega}} \|\mathbf{v}_h\|_{\mathbb{R}^{N_\omega}}. \quad (7.3)$$

We choose as matrix norm the ∞ -norm. The matrix \mathbf{M}^{-1} can be written

$$\mathbf{M}^{-1} = \begin{pmatrix} \tilde{\mathbf{I}} & \mathbf{0} \\ -\frac{\tilde{\mathbf{w}}}{w_{N_\omega}} & 1 \end{pmatrix} = \begin{pmatrix} \tilde{\mathbf{I}} & \mathbf{0} \\ \mathbf{0} & \frac{1}{w_{N_\omega}} \end{pmatrix} \begin{pmatrix} \tilde{\mathbf{I}} & \mathbf{0} \\ -\tilde{\mathbf{w}} & w_{N_\omega} \end{pmatrix} \quad (7.4)$$

$$\|\mathbf{M}^{-1}\|_{\infty} \leq \max \left\{ 1, \frac{1}{|w_{N_\omega}|} \right\} \max \{1, \|\mathbf{w}\|_1\}.$$

Equation (7.1) comes from the equivalence between $\|\mathbf{w}\|_1$ and $\|\mathbf{w}\|_{\infty}$ in which appears the dimension N_ω that is bounded by the assumption of a bounded number of element in each patch ω . \square

A possible algorithm for the construction of the patches can be set up quite easily for $k \geq 2$, resorting to the presence of basis functions whose support is contained in the polygonal elements.

In the following we numerically investigate the value of the stability factor in the case of Test 1 (Section 5.1). Namely, we devise a simple possible strategy to build a set of patches that minimizes the stability constant and apply it to different families of progressively refined meshes. We then compute the maximum stability constant for each one of the resulting constructed sets and then consider its behaviour with respect to refinement, VEM order and mesh quality.

For a given patch $\omega \in \mathcal{T}_{h,\omega}$ let us define the smallest stability constant

$$C_{\mathcal{S}_h^\omega} = \max \left\{ 1, \frac{1}{|w_r|} \right\}, \quad (7.5)$$

corresponding to all the possible choices of the internal dofs as the dof satisfying (3.3) used to impose (3.4). In order to construct patches we start computing the stability constant for each basis function considering as patch its support. Then, a first set of possible patches is built applying a greedy approach. We sort the stability constants in an increasing order and we start to select the patches choosing

Table 19: **Test 1, order 2** Behaviour of the maximum stability constants of the patches built as described in Section 7, and percentage of patches with only one polygon.

distorted square mesh			distorted Voronoi mesh			highly distorted Voronoi mesh		
h	$C_{S_h^\omega}$	%	h	$C_{S_h^\omega}$	%	h	$C_{S_h^\omega}$	%
0.0161	1.03	99.9	0.0266	1.81	13.3	0.0621	2.35	11.6
0.0194	1.00	99.9	0.0308	1.64	15.5	0.0718	2.10	13.0
0.0243	1.00	99.7	0.0357	1.39	17.6	0.0822	1.91	14.8
0.0321	1.00	99.6	0.0423	1.19	21.2	0.0962	1.67	16.0
0.0475	1.00	99.0	0.0542	1.00	0.1	0.1217	1.00	0.1
0.0933	1.00	99.1	0.0711	1.00	0.1	0.1547	1.00	0.1

the support of the basis functions with smallest stability constant that do not contain in the support elements already included in a patch. Every time we create a patch, we mark the elements around it as elements possibly included in this patch if not included by the process in a different patch. We end the process when all the elements are included in a patch or marked as candidates to be included in a neighboring patch. In a second step we consider the created patches with the largest stability constants for a possible gluing with neighboring patches and elements marked for gluing, considering if this gluing can reduce the stability constant. In this gluing step we consider all the basis functions that become internal after the gluing and compute for all of them the stability constant of the patch and set as stability constant of the new patch the smallest one.

In Tables 19-21 we show the maximum values of constants $C_{S_h^\omega}$ obtained with this process on different meshes for the test in Section 5.1 and different VEM orders k . In Table 19 we report the value of the computed stability constants and the percentage of the patches that are constituted by one polygon for $k = 2$, meaning that the function φ_r is one of the internal basis functions. We can observe that the estimated stability constants can be considered quite stable with respect to refinement and mesh quality. In Table 20 we report the same data for $k = 3$, and the previous conclusions are confirmed in an even more clear way. Results reported for $k = 3$ are obtained with no gluing step. This confirms the assumption that the presence of several internal basis functions simplifies the construction of patches satisfying condition (4) in Definition 3.1. Finally, in Table 21 we report the outcome of the algorithm for $k = 1$. The stability of the projection operator S_h^ω corresponding to the patches given by the previous algorithm with respect to mesh refinement and patch changes is less evident. A different strategy that considers from the beginning patches with a number of internal basis functions larger than one could probably yield better results.

Table 20: **Test 1, order 3** Behaviour of the maximum stability constants of the patches built as described in Section 7, and percentage of patches with only one polygon.

distorted square mesh			distorted Voronoi mesh			highly distorted Voronoi mesh		
h	$C_{S_h^\omega}$	%	h	$C_{S_h^\omega}$	%	h	$C_{S_h^\omega}$	%
0.0194	1.00	100.0	0.0266	1.00	22.2	0.0621	1.00	79.3
0.0243	1.00	100.0	0.0308	1.00	24.5	0.0718	1.00	82.5
0.0321	1.00	100.0	0.0357	1.00	35.9	0.0822	1.00	87.3
0.0475	1.00	100.0	0.0423	1.00	32.3	0.0962	1.00	90.6
0.0933	1.00	100.0	0.0542	1.00	31.9	0.1217	1.00	96.6
0.1784	1.00	100.0	0.0711	1.00	52.4	0.1547	1.00	100.0

Table 21: **Test 1, order 1** Behaviour of the maximum stability constants of the patches built as described in Section 7.

distorted square mesh		distorted Voronoi mesh		highly distorted Voronoi mesh	
h	$C_{S_h^\omega}$	h	$C_{S_h^\omega}$	h	$C_{S_h^\omega}$
0.0161	8.41e+01	0.0266	2.12e+02	0.0621	6.53e+01
0.0194	5.64e+02	0.0308	1.57e+02	0.0718	4.32e+01
0.0243	1.25e+01	0.0357	8.82e+01	0.0822	4.45e+01
0.0321	1.82	0.0423	7.81e+01	0.0962	4.34e+01
0.0475	1.53	0.0542	4.71e+01	0.1217	8.71e+01
0.0933	1.06	0.0711	3.60e+01	0.1547	9.21e+00

Acknowledgments

The authors wish to thank Matías Fernando Benedetto for his precious help in developing the code that was used for numerical simulations.

Bibliography

1. P. M. Adler. *Fractures and Fracture Networks*. Kluwer Academic, Dordrecht, 1999.
2. B. Ahmad, A. Alsaedi, F. Brezzi, L.D. Marini, and A. Russo. Equivalent projectors for virtual element methods. *Computers & Mathematics with Applications*, 66:376–391, September 2013.
3. M. Ainsworth and J.T. Oden. A unified approach to a posteriori error estimation using element residual methods. *Numer. Math.*, 65(1):23–50, 1993.
4. G. Akrivis, C. Makridakis, and R.H. Nochetto. A posteriori error estimates for the Crank-Nicolson method for parabolic equations. *Math. Comp.*, 75(254):511–531, 2006.
5. P. F. Antonietti, L. Beirão da Veiga, D. Mora, and M. Verani. A stream virtual element formulation of the Stokes problem on polygonal meshes. *SIAM J. Numer. Anal.*, 52(1):386–404, 2014.
6. I. Babuška and W.C. Rheinboldt. Error estimates for adaptive finite element compu-

- tations. *SIAM J. Numer. Anal.*, 15(4):736–754, 1978.
7. R. Becker and R. Rannacher. A feed-back approach to error control in finite element methods: basic analysis and examples. *East-West J. Numer. Math.*, 4(4):237–264, 1996.
 8. L. Beirão da Veiga, F. Brezzi, A. Cangiani, G. Manzini, L.D. Marini, and A. Russo. Basic principles of virtual element methods. *Mathematical Models and Methods in Applied Sciences*, 23(01):199–214, 2013.
 9. L. Beirão da Veiga, F. Brezzi, L.D. Marini, and A. Russo. The hitchhiker’s guide to the virtual element method. *Math. Models Methods Appl. Sci.*, 24(8):1541–1573, 2014.
 10. L. Beirão da Veiga, F. Brezzi, L.D. Marini, and A. Russo. Virtual element methods for general second order elliptic problems on polygonal meshes. *Mathematical Models and Methods in Applied Sciences*, 2015.
 11. L. Beirão da Veiga, K. Lipnikov, and G. Manzini. *The Mimetic Finite Difference Method for Elliptic Problems*, volume 11 of *Modeling, Simulation & Applications*. Springer, 2014.
 12. L. Beirão da Veiga, C. Lovadina, and D. Mora. A virtual element method for elastic and inelastic problems on polytope meshes. *Comput. Methods Appl. Mech. Engrg.*, 295:327–346, 2015.
 13. L. Beirão da Veiga, C. Lovadina, and A. Russo. Stability Analysis for the Virtual Element Method. *ArXiv e-prints*, July 2016.
 14. L. Beirão da Veiga and G. Manzini. Residual a posteriori error estimation for the virtual element method for elliptic problems. *ESAIM: Mathematical Modelling and Numerical Analysis*, 49(2):577–599, 2015.
 15. M.F. Benedetto, S. Berrone, A. Borio, S. Pieraccini, and S. Scialò. A hybrid mortar virtual element method for discrete fracture network simulations. *J. Comput. Phys.*, 306:148–166, 2016.
 16. M.F. Benedetto, S. Berrone, A. Borio, S. Pieraccini, and S. Scialò. Order preserving SUPG stabilization for the virtual element formulation of advection-diffusion problems. *Comput. Methods Appl. Mech. Engrg.*, 311:18 – 40, 2016.
 17. M.F. Benedetto, S. Berrone, S. Pieraccini, and S. Scialò. The virtual element method for discrete fracture network simulations. *Comput. Methods Appl. Mech. Engrg.*, 280(0):135 – 156, 2014.
 18. M.F. Benedetto, S. Berrone, and S. Scialò. A globally conforming method for solving flow in discrete fracture networks using the virtual element method. *Finite Elem. Anal. Des.*, 109:23–36, 2016.
 19. C. Bernardi and R. Verfürth. Adaptive finite element methods for elliptic equations with non-smooth coefficients. *Numerische Mathematik*, 85(4):579–608, 2000.
 20. S. Berrone. Adaptive discretization of stationary and incompressible Navier-Stokes equations by stabilized finite element methods. *Comput. Methods Appl. Mech. Engrg.*, 190(34):4435–4455, 2001.
 21. S. Berrone. Robust a posteriori error estimates for finite element discretizations of the heat equation with discontinuous coefficients. *ESAIM: Mathematical Modelling and Numerical Analysis*, 40(06):991–1021, 2006.
 22. S. Berrone. A local-in-space-timestep approach to a finite element discretization of the heat equation with a posteriori estimates. *SIAM Journal on Numerical Analysis*, 47(4):3109–3138, 2009.
 23. S. Berrone. Skipping transition conditions in a posteriori error estimates for finite element discretizations of parabolic equations. *M2AN Math. Model. Numer. Anal.*, 44(3):455–484, 2010.
 24. S. Berrone and A. Borio. Orthogonal polynomials in badly shaped polygonal elements

- for the Virtual Element Method. *Finite Elements in Analysis & Design*, 129:14–31, 2017.
25. S. Berrone, A. Borio, and S. Scialò. A posteriori error estimate for a PDE-constrained optimization formulation for the flow in DFNs. *SIAM J. Numer. Anal.*, 54(1):242–261, 2016.
 26. S. Berrone and T. Kozubek. An adaptive wem algorithm for solving elliptic boundary value problems in fairly general domains. *SIAM Journal on Scientific Computing*, 28(6):2114–2138, 2006.
 27. S. Berrone and M. Marro. Space-time adaptive simulations for unsteady Navier-Stokes problems. *Comput. & Fluids*, 38(6):1132–1144, 2009.
 28. S. Berrone, S. Pieraccini, and S. Scialò. A PDE-constrained optimization formulation for discrete fracture network flows. *SIAM J. Sci. Comput.*, 35(2):B487–B510, 2013.
 29. S. Berrone, S. Pieraccini, and S. Scialò. Towards effective flow simulations in realistic discrete fracture networks. *J. Comput. Phys.*, 310:181–201, 2016.
 30. S. Berrone, S. Pieraccini, S. Scialò, and F. Vicini. A parallel solver for large scale DFN flow simulations. *SIAM J. Sci. Comput.*, 37(3):C285–C306, 2015.
 31. S. Berrone and E. Süli. Two-sided a posteriori error bounds for incompressible quasi-Newtonian flows. *IMA J. Numer. Anal.*, 28(2):382–421, 2008.
 32. P. Binev, W. Dahmen, and R. DeVore. Adaptive finite element methods with convergence rates. *Numer. Math.*, 97(2):219–268, 2004.
 33. F. Brezzi, A. Buffa, and K. Lipnikov. Mimetic finite differences for elliptic problems. *ESAIM: Mathematical Modelling and Numerical Analysis*, 43:277–295, 2009.
 34. A. Cangiani, E. H. Georgoulis, T. Pryer, and O. J. Sutton. A posteriori error estimates for the virtual element method. Available online at <http://adsabs.harvard.edu/abs/2016arXiv160305855C>, 2016.
 35. A. Cangiani, G. Manzini, and O.J. Sutton. Conforming and nonconforming virtual element methods for elliptic problems. 2016.
 36. L. Diening, C. Kreuzer, and R. Stevenson. Instance optimality of the adaptive maximum strategy. *Foundations of Computational Mathematics*, pages 1–36, 2015.
 37. V. Dolejší, A. Ern, and M. Vohralík. A framework for robust a posteriori error control in unsteady nonlinear advection-diffusion problems. *SIAM J. Numer. Anal.*, 51(2):773–793, 2013.
 38. M. Dryja, V.M. Sarkis, and B.O. Widlund. Multilevel schwarz methods for elliptic problems with discontinuous coefficients in three dimensions. *Numerische Mathematik*, 72(3):313–348, 1996.
 39. A. Ern and M. Vohralík. Flux reconstruction and a posteriori error estimation for discontinuous Galerkin methods on general nonmatching grids. *C. R. Math. Acad. Sci. Paris*, 347(7-8):441–444, 2009.
 40. P. Jiránek, Z. Strakoš, and M. Vohralík. A posteriori error estimates including algebraic error and stopping criteria for iterative solvers. *SIAM J. Sci. Comput.*, 32(3):1567–1590, 2010.
 41. M. Petzoldt. A posteriori error estimators for elliptic equations with discontinuous coefficients. *Advances in Computational Mathematics*, 16(1):47–75, 2002.
 42. B. Riviere and M.F. Wheeler. A posteriori error estimates for a discontinuous galerkin method applied to elliptic problems. *Computers & Mathematics with Applications*, 46(1):141 – 163, 2003.
 43. R. Stevenson. Optimality of a standard adaptive finite element method. *Found. Comput. Math.*, 7(2):245–269, 2007.
 44. C. Talischi, G.H. Paulino, A. Pereira, and I.F.M. Menezes. Polymesh: a general-purpose mesh generator for polygonal elements written in matlab. *Structural and*

- Multidisciplinary Optimization*, 45(3):309–328, 2012.
45. R. Verfürth. A posteriori error estimation and adaptive mesh-refinement techniques. *Journal of Computational and Applied Mathematics*, 50:67–83, 1994.
 46. R. Verfürth. *A Review of a Posteriori Error Estimation and Adaptive Mesh-Refinement Techniques*. Advances in Numerical Mathematics Series. Teubner B.G. GmbH, 1996.
 47. R. Verfürth. A posteriori error estimates for finite element discretizations of the heat equation. *Calcolo*, 40(3):195–212, 2003.
 48. M. Vohralík. A posteriori error estimates for lowest-order mixed finite element discretizations of convection-diffusion-reaction equations. *SIAM Journal on Numerical Analysis*, 45(4):1570–1599, 2007.
 49. J. Wang. Superconvergence analysis for finite element solutions by the least-squares surface fitting on irregular meshes for smooth problems. *J. Math. Study*, 33(3):229–243, 2000.
 50. T. Zhang and L. Tang. Superconvergence of the stable $P_1 - P_1$ finite element pair for Stokes problem. *Calcolo*, pages 1–15, 2015.
 51. O. C. Zienkiewicz and J. Z. Zhu. The superconvergent patch recovery and a posteriori error estimates. part 2: Error estimates and adaptivity. *International Journal for Numerical Methods in Engineering*, 33(7):1365–1382, 1992.